

HEAVY QUARK PAIR PRODUCTION NEAR THRESHOLD WITH  
POTENTIAL NON-RELATIVISTIC QCDAntonio Pineda<sup>1a</sup> and Adrian Signer<sup>b</sup>

<sup>a</sup> *Dept. d'Estructura i Constituents de la Matèria  
U. Barcelona, Diagonal 647, E-08028 Barcelona, Catalonia, Spain*

<sup>b</sup> *Institute for Particle Physics Phenomenology  
Durham, DH1 3LE, England*

**Abstract**

We study the effect of the resummation of logarithms for  $t\bar{t}$  production near threshold and inclusive electromagnetic decays of heavy quarkonium. This analysis is complete at next-to-next-to-leading order and includes the full resummation of logarithms at next-to-leading-logarithmic accuracy and some partial contributions at next-to-next-to-leading logarithmic accuracy. Compared with fixed-order computations at next-to-next-to-leading order the scale dependence and convergence of the perturbative series is greatly improved for both the position of the peak and the normalization of the total cross section. Nevertheless, we identify a possible source of large scale dependence in the result. At present we estimate the remaining theoretical uncertainty of the normalization of the total cross section to be of the order of 10% and for the position of the peak of the order of 100 MeV.

---

<sup>1</sup>Permanent address after September 1st: Grup de Física Teòrica and IFAE, Universitat Autònoma de Barcelona, E-08193 Bellaterra, Barcelona, Spain.

# 1 Introduction

The existence of (heavy) quarks with a large mass compared with  $\Lambda_{QCD}$ , like the top, the bottom, and maybe the charm, makes particularly interesting the study of physical processes where a heavy quark pair is created close to threshold, because accurate experimental information over the whole near-threshold region may allow for a precise determination of some parameters of the Standard Model. For instance, the future International Linear Collider (ILC) offers the opportunity to study the top quark with unprecedented accuracy [1, 2, 3]. To fully exploit the potential of an ILC in this respect, it is essential that a dedicated measurement of the cross section for the production of a top antitop quark pair close to threshold is made. Such a threshold scan allows for an extremely precise measurement of the top-quark mass and yields information on the top-quark width and the top-Higgs Yukawa coupling. The analogous threshold scan for the  $b\bar{b}$  sector is also fundamental for non-relativistic sum rules [4, 5, 6, 7, 8] and may lead to accurate determinations of the bottom quark mass [9].

The characteristic feature of heavy-quark pair production close to threshold is the smallness of the relative velocity  $v$  of the heavy quarks in the centre of mass frame. This entails a hierarchy of scales  $\mu_h \gg \mu_s \gg \mu_{us}$  where the hard scale  $\mu_h$  is of the order of the heavy quark mass  $m$ , the soft scale  $\mu_s \sim mv$  is of the order of the typical momentum of the heavy quarks and the ultrasoft scale  $\mu_{us} \sim mv^2$  is of the order of the typical kinetic energy of the heavy quarks. The presence of an additional small parameter can be exploited by systematically expanding in the strong coupling  $\alpha_s$  and  $v$ . Thus, in this context, a next-to-leading order (NLO) calculation takes into account all terms that are suppressed by either  $\alpha_s$  or  $v$  relative to the leading-order (LO) result, whereas a next-to-next-to-leading order (NNLO) calculation includes all terms suppressed by two powers of the small parameter  $\alpha_s \sim v$ . The coefficients of this perturbative series contain large logarithms  $\log v$ . In order to improve the reliability of the calculation, these logarithms should be resummed. Counting  $\alpha \log v \sim 1$  in a NLO or NNLO calculation produces a result of next-to-leading logarithmic (NLL) or next-to-next-to-leading logarithmic (NNLL) accuracy respectively. There are no leading logarithmic (LL) corrections, thus the LO and LL results are the same.

The expansion as well as the resummation of the logarithms can be organized most efficiently by using an effective theory (for a review see Ref. [10]) approach. This is done most conveniently by using the threshold expansion [11] that allows to separate the full result of an integral into contributions due to the various modes. Denoting the generic integration momentum by  $k = (k^0, \mathbf{k})$ , the modes that are relevant are: the hard mode  $k^0 \sim \mathbf{k} \sim \mu_h$ , the soft mode  $k^0 \sim \mathbf{k} \sim \mu_s$ , the potential mode  $k^0 \sim \mu_{us}, \mathbf{k} \sim \mu_s$  and the ultrasoft mode  $k^0 \sim \mathbf{k} \sim \mu_{us}$ . The standard procedure is to first match QCD to non-relativistic QCD (NRQCD) [12] at the hard scale. This corresponds to integrating out the hard

modes using the threshold expansion. The resulting theory is then matched to potential NRQCD (pNRQCD) [13, 14] by integrating out the soft modes and potential gluon modes. At this stage the theory consists of a non-relativistic quark pair interacting through potentials and ultrasoft gluons.

Within this framework NNLO calculations have been performed by several groups (for a review in the case of the top quark see [3]) and quite a few partial results needed for a NNNLO calculation have been obtained [15, 16, 17, 18, 19, 20, 21]. Moreover, the existence of the effective theory also provides the necessary framework on which to use renormalization group (RG) techniques. These allow to resum the large logarithms,  $\log v$ , that appear as the ratio of the different scales appearing in the physical system:  $\log \mu_h/\mu_s$  and  $\log \mu_s/\mu_{us}$ . At present, the situation is as follows. The computation of the heavy quarkonium spectrum is known with NNLL accuracy [22, 23] (for the hyperfine splitting at NNNLL [24, 25]). Inclusive electromagnetic decays of heavy quarkonium have been computed to NLL [26, 23] and for the spin-zero, spin-one ratio to NNLL [27]. In the case of top-quark pair production a renormalization-group improved (RGI) calculation is available [28, 29], using a somewhat different approach, referred to as vNRQCD [30] (in this theory, soft degrees of freedom are kept dynamical and the matching from QCD to vNRQCD is carried out directly). However, so far, there is no RGI calculation of heavy-quark pair production within the conventional pNRQCD approach. It is the main purpose of this work to close this gap and to provide the ingredients to perform such computations in the case of top and bottom-quark pair production. We will report results on  $t\bar{t}$  production near threshold, as well as elaborate on the computation of non-relativistic sum rules presented in Ref. [9]. Inclusive electromagnetic decays of heavy quarkonium will also be considered. These analyses will be complete at NNLO and include the complete resummation of logarithms at NLL accuracy and some partial contributions at NNLL.

The importance of higher order logarithms can be illustrated in the top quark case. In the on-shell scheme, the NNLO corrections turned out to be much larger than anticipated and, moreover, made the theoretical prediction very strongly scale dependent. If the cross section is expressed in terms of a threshold mass [31, 32, 33] rather than the pole mass, the position of its peak is more stable and can be predicted with a small theoretical error. This will allow to determine the top threshold mass and ultimately the top  $\overline{\text{MS}}$ -mass with a very small error. The situation is much less favourable regarding the normalization of the cross section. The corrections are huge and the scale dependence at NNLO is larger than at NLO, indicating that this quantity is not well under control at NNLO. This affects how accurately one may obtain the top-quark width and the top-Higgs Yukawa coupling. It has been shown that the inclusion of the potentially large  $\log v$  terms is numerically very important and improves the situation regarding the normalization of the cross section considerably [28, 29]. One of the aims of

this paper is to compare with these results. We also investigate to what extent the resummation of the logarithms is really required and to what extent the improvement we observe in the RGI results is simply due to the partial inclusion of higher-order terms. To do so we will produce “NNNLO” results by re-expanding full RGI results and dropping terms that are beyond NNNLO. Of course, these results are by no means complete at NNNLO, but they contain those NNNLO terms that are enhanced by a logarithm. To obtain an estimate of the importance of resummation, we then compare these “NNNLO” curves to the full RGI results. As we will see, this partial inclusion of NNNLO terms does reproduce the bulk of the RGI result except for rather small values of  $\mu_s$ . In particular, in the case of the top quark the difference between fully resummed and partial NNNLO results is small.

The paper is structured as follows: In Section 2 we present our formalism and describe how to perform a RGI calculations in pNRQCD. Some formulae and technical details of this section are relegated to the Appendix. In Section 3 we apply these results to  $t\bar{t}$  production near threshold. Section 4 contains the application to bottomonium non-relativistic sum rules and inclusive electromagnetic decay widths. In the final section, we show our conclusions.

## 2 Effective theory

Within pNRQCD,  $\psi$  and  $\chi$ , the fields representing the non-relativistic quark and antiquark, interact through a potential and with dynamical ultrasoft gluons. It is well known that the leading Coulomb interaction is not suppressed and has to be included in the LO Lagrangian which is given by

$$\begin{aligned} \mathcal{L}_{\text{pNRQCD}}^{(0)} &= \psi^\dagger \left( i\partial^0 + \frac{\partial^2}{2m} \right) \psi + \chi^\dagger \left( i\partial^0 - \frac{\partial^2}{2m} \right) \chi \\ &+ \int d^3\mathbf{r} \left( \psi^\dagger T^a \psi \right) \left( -\frac{\alpha_s}{r} \right) \left( \chi^\dagger T^a \chi \right), \end{aligned} \quad (1)$$

where  $T^a$  are the colour matrices and the strong coupling is understood to be evaluated at the soft scale,  $\alpha_s \equiv \alpha_s(\mu_s)$ , unless explicitly indicated otherwise. Subleading effects are incorporated in the Lagrangian as corrections to the potential,  $\delta V$ , and as interactions of the heavy quarks with ultrasoft gluons. For further details we refer to Ref. [10]. If we restrict the accuracy of our analysis to NNLL, ultrasoft gluons do not appear as physical final states (though their effect is embedded in the RGI running of the matching coefficients of the potentials and currents). It follows that the number of particles is conserved (we only have one heavy quark and one heavy antiquark) and the problem effectively becomes equivalent to do standard quantum mechanics perturbation theory. If we restrict

ourselves to study the Hilbert space spanned by the heavy quark-antiquark system in the singlet colour sector we are lead to solve the following equation for the associated Green function

$$(H(\mathbf{r}, \mathbf{p}) - E)G(\mathbf{r}, \mathbf{r}'; E) = \delta(\mathbf{r} - \mathbf{r}'), \quad (2)$$

where

$$H = H_c + \delta V \quad (3)$$

and

$$H_c = \frac{\mathbf{p}^2}{m} - C_F \frac{\alpha_s}{r}, \quad (4)$$

with  $C_F = (N_c^2 - 1)/(2N_c)$  (where the colour factor  $N_c = 3$ ). The explicit expression of  $\delta V$  (the correction to the Coulomb potential) will be given afterwards. The full Green function  $G$  can be solved iteratively in an expansion in the velocity by performing multiple insertions of  $\delta V$ . The LO solution is the Coulomb Green function  $G_c$  and we write

$$G(\mathbf{r}, \mathbf{r}'; E) = G_c(\mathbf{r}, \mathbf{r}'; E) + \delta G(\mathbf{r}, \mathbf{r}'; E), \quad (5)$$

where

$$G_c(\mathbf{r}, \mathbf{r}'; E) = \langle \mathbf{r} | \frac{1}{H_c - E} | \mathbf{r}' \rangle \quad (6)$$

and

$$\delta G(\mathbf{r}, \mathbf{r}'; E) = -\langle \mathbf{r} | \frac{1}{H_c - E} \delta V \frac{1}{H_c - E} | \mathbf{r}' \rangle + \dots \quad (7)$$

$G(\mathbf{r}, \mathbf{r}'; E)$  is related to the correlators that appear in the total cross section for the production of a heavy quark pair,  $\sigma(e^+e^- \rightarrow Q\bar{Q})$  with the centre of mass energy  $\sqrt{q^2} = \sqrt{s} \sim 2m$ . This is the key quantity we are interested in. The cross section obtains contributions from  $\gamma$  and  $Z$  exchange. In order to simplify the discussion we ignore the  $Z$  exchange in what follows. The cross section can then be written as

$$\sigma^\gamma(s) = \frac{4\pi\alpha_{\text{EM}}^2}{3s} e_Q^2 R(s), \quad (8)$$

where  $e_Q$  is the electric charge of the heavy quark,  $\alpha_{\text{EM}}$  the electromagnetic coupling at the hard scale and the ratio  $R \equiv \sigma(e^+e^- \rightarrow Q\bar{Q})/\sigma(e^+e^- \rightarrow \mu^+\mu^-)$  is expressed as a correlator of two heavy-quark vector currents  $j^\mu(x) \equiv \bar{Q}\gamma^\mu Q(x)$

$$R(s) = \frac{4\pi}{s} \text{Im} \left( -i \int d^4x e^{iq \cdot x} \langle 0 | T \{ j^\mu(x) j_\mu(0) \} | 0 \rangle \right). \quad (9)$$

In order to compute this correlator, we first express the current in terms of the non-relativistic two-component spinor fields  $\psi^\dagger$  and  $\chi$ ,

$$\bar{Q}\gamma^\mu Q = c_1 \chi^\dagger \sigma^i \psi - \frac{d_1}{6m^2} \chi^\dagger \sigma^i (i\mathbf{D})^2 \psi + \dots, \quad (10)$$

where the matching coefficients  $c_1$  and  $d_1$  are normalized to 1 at LO. By using the equations of motion, Eq. (10) can also be written in the following way

$$\bar{Q}\gamma^\mu Q = c_1\chi^\dagger\sigma^i\psi - \frac{d_1}{6m}i\partial_0(\chi^\dagger\sigma^i\psi) + \dots. \quad (11)$$

Given the Lagrangian, we solve the corresponding Schrödinger equation and ultimately relate the imaginary part of the spin one Green function at the origin to  $R(s)$  by the equality

$$R(E) = \frac{24\pi e_Q^2 N_c}{s} \left( c_1^2 - c_1 d_1 \frac{E}{3m} \right) \text{Im} G_{s=1}(\mathbf{0}, \mathbf{0}; E), \quad (12)$$

which is valid with NNLL accuracy (where  $E \equiv \sqrt{s} - 2m$ ). We note that in evaluating  $R(E)$  we expand the expression in Eq. (12) and drop all terms that are beyond NNLO/NNLL. In particular, we set  $c_1 = 1$  in the second term of the parenthesis.

In order to connect with the notation in Ref. [10], Eq. (12) can also be written as

$$R(E) = \frac{18N_c}{m^2\alpha_{\text{EM}}^2} \text{Im} G_{s=1}(\mathbf{0}, \mathbf{0}; E) \left[ \text{Im} f_{\text{EM}}^{\text{pNR}}({}^3S_1) + \text{Im} g_{\text{EM}}^{\text{pNR}}({}^3S_1) \frac{E}{m} \right], \quad (13)$$

with

$$\begin{aligned} \text{Im} f_{\text{EM}}^{\text{pNR}}({}^3S_1) &= \frac{\pi e_Q^2 \alpha_{\text{EM}}^2}{3} c_1^2, \\ \text{Im} g_{\text{EM}}^{\text{pNR}}({}^3S_1) &= -\frac{\pi e_Q^2 \alpha_{\text{EM}}^2}{3} c_1 \left( c_1 + \frac{1}{3} d_1 \right). \end{aligned} \quad (14)$$

## 2.1 Potential

The computation of  $G(\mathbf{0}, \mathbf{0}; E)$  will lead to divergences. These divergences are regularized by performing all calculations in momentum space [34] and using dimensional regularisation in  $D = d + 1 = 4 - 2\epsilon$  dimensions. Thus, the LO Green function at the origin, Eq. (6), is understood as

$$G_c(\mathbf{r}, \mathbf{r}'; E) \Big|_{\mathbf{r}=\mathbf{r}'=\mathbf{0}} \equiv \int \frac{d^d \mathbf{p}}{(2\pi)^d} \frac{d^d \mathbf{p}'}{(2\pi)^d} \tilde{G}_c(\mathbf{p}, \mathbf{p}'; E), \quad (15)$$

where  $\tilde{G}$  denotes the Fourier transform of the Green function and the insertions, Eq. (7), are to be evaluated as indicated in Eqs. (42) and (43). Using the threshold expansion [11], the Fourier transform of the leading order Green function can be

computed as the sum of all ladder diagrams with the exchange of potential gluons between the heavy quarks and can be written as

$$\begin{aligned} \tilde{G}_c(\mathbf{p}, \mathbf{p}'; E) &= (2\pi)^d \delta^{(d)}(\mathbf{p} - \mathbf{p}') \frac{-1}{E - \mathbf{p}^2/m} \\ &+ \frac{4\pi C_F \alpha_s}{(E - \mathbf{p}^2/m)(\mathbf{p} - \mathbf{p}')^2 (E - \mathbf{p}'^2/m)} + \text{finite}, \end{aligned} \quad (16)$$

where we have omitted terms that are finite if Eq. (16) is used in Eq. (15). The Green function at the origin has a ultraviolet divergence that manifests itself as a pole  $1/\epsilon$ . Using  $\overline{\text{MS}}$  subtraction and then taking the limit  $\epsilon \rightarrow 0$  we find [34, 35]

$$G_c(\mathbf{0}, \mathbf{0}; E) = -\frac{\alpha_s C_F m^2}{4\pi} \left( \frac{1}{2\lambda} + \frac{1}{2} \log \frac{-4mE}{\mu_s^2} - \frac{1}{2} + \gamma_E + \psi(1 - \lambda) \right) \quad (17)$$

where  $\lambda \equiv C_F \alpha_s / (2\sqrt{-E/m})$ .

Higher-order corrections to the Green function can be computed perturbatively in two steps. First, the pNRQCD Lagrangian has to be determined to the accuracy needed for the calculation. Second, higher-order corrections are computed using quantum mechanics perturbation theory, Eq. (7). Since some of the potentials generate singularities in insertions, we have to start from the NNLO potential computed in  $D$  dimensions [34]. It is essential to manipulate the potential consistently in  $D$  dimensions, since it allows us to use the same hard matching coefficients defined in the  $\overline{\text{MS}}$ -scheme obtained in Refs. [36, 37]. We then bring the potential in a form that is more suitable to be combined with the RGI coefficients as presented in Ref. [22]. In particular we use

$$\begin{aligned} &\frac{C_F \pi \alpha_s}{m^2} \int \prod_{i=1}^4 \frac{d^d \mathbf{p}_i}{(2\pi)^d} \tilde{G}_c(\mathbf{p}_1, \mathbf{p}_2) \left( \frac{\mathbf{p}_2^2 - \mathbf{p}_3^2}{(\mathbf{p}_2 - \mathbf{p}_3)^2} \right)^2 \tilde{G}_c(\mathbf{p}_3, \mathbf{p}_4) \\ &= \frac{C_F^2}{2} (1 - 2\epsilon) \frac{e^{\epsilon \gamma_E} \Gamma^2(\frac{1}{2} - \epsilon) \Gamma(\frac{1}{2} + \epsilon)}{\pi^{3/2} \Gamma(1 - 2\epsilon)} \times \\ &\quad \int \prod_{i=1}^4 \frac{d^d \mathbf{p}_i}{(2\pi)^d} \tilde{G}_c(\mathbf{p}_1, \mathbf{p}_2) \frac{\pi^2 \alpha_s^2 \mu_s^{2\epsilon}}{m |\mathbf{p}_2 - \mathbf{p}_3|^{1+2\epsilon}} \tilde{G}_c(\mathbf{p}_3, \mathbf{p}_4) \end{aligned} \quad (18)$$

to eliminate the  $C_F^2$  term of the non-analytic potential  $1/q^{1+2\epsilon}$ , present in Ref. [34]. The angular momentum operator is generalized to

$$\frac{\mathbf{L}^2}{2\pi r^3} \rightarrow \left( \frac{\mathbf{p}^2 - \mathbf{p}'^2}{\mathbf{q}^2} \right)^2 - 1 \quad (19)$$

to be compatible with  $D$  dimensional calculations in momentum space. Note that an insertion of this operator does not vanish even for an  $S$ -wave (see Eq. (86)),

but the corresponding contribution could be absorbed into a redefinition of the matching coefficient of the current.

At NNLL, the higher-order corrections to the  $D$ -dimensional potential in momentum space,  $\delta\tilde{V}$ , can then be written as

$$\begin{aligned}
\delta\tilde{V} = & -c_4 \frac{\mathbf{P}^4}{4m^3} (2\pi)^d \delta^{(d)}(\mathbf{q}) - 4\pi C_F \frac{\alpha_{\tilde{V}_s}}{\mathbf{q}^2} + 4\pi C_F \frac{\alpha_s}{\mathbf{q}^2} \\
& - C_F C_A D_s^{(1)} \frac{\pi^2 \mu_s^{2\epsilon}}{m q^{1+2\epsilon}} (1-\epsilon) \frac{e^{\epsilon\gamma_E} \Gamma^2(\frac{1}{2}-\epsilon) \Gamma(\frac{1}{2}+\epsilon)}{\pi^{3/2} \Gamma(1-2\epsilon)} \\
& - \frac{2\pi C_F D_{1,s}^{(2)} \mathbf{p}^2 + \mathbf{p}'^2}{m^2 \mathbf{q}^2} + \frac{\pi C_F D_{2,s}^{(2)}}{m^2} \left( \left( \frac{\mathbf{p}^2 - \mathbf{p}'^2}{\mathbf{q}^2} \right)^2 - 1 \right) \\
& + \frac{3\pi C_F D_{d,s}^{(2)}}{m^2} - \frac{4\pi C_F D_{S^2,s}^{(2)}}{d m^2} [\mathbf{S}_1^i, \mathbf{S}_1^j] [\mathbf{S}_2^i, \mathbf{S}_2^j] \\
& + \frac{4\pi C_F D_{S_{12},s}^{(2)}}{d m^2} [\mathbf{S}_1^i, \mathbf{S}_1^r] [\mathbf{S}_2^i, \mathbf{S}_2^j] \left( \delta^{rj} - d \frac{q^r q^j}{q^2} \right) \\
& - \frac{6\pi C_F D_{LS,s}^{(2)}}{m^2} \frac{p^i q^j}{q^2} \left( [\mathbf{S}_1^i, \mathbf{S}_1^j] + [\mathbf{S}_2^i, \mathbf{S}_2^j] \right),
\end{aligned} \tag{20}$$

where the colour factor  $C_A = N_c$ ,  $\mathbf{q} = \mathbf{p} - \mathbf{p}'$  and  $\alpha_{\tilde{V}_s}$  contains the corrections to the static potential up to NNLL [38, 39]. We will set  $c_4 = 1$  due to reparameterization invariance. We would like to stress that the Wilson coefficients are not dimensionless in  $D \neq 4$ .

The non-relativistic reduction of the spin operators of the potential depends on the operators used to single out the physical state we want to study. In our case we are using the vector currents, which project to the spin-one state. We also have to be careful to use the same conventions than those used to obtain the hard piece of the matching coefficients. This produces  $O(\epsilon)$  terms multiplying the  $\mathbf{S}^2$  operator. In practise one can do the following replacement for the  $\mathbf{S}^2$  operator with  $\mathbf{S}^2 = 2$

$$- \frac{4\pi C_F D_{S^2,s}^{(2)}}{d m^2} [\mathbf{S}_1^i, \mathbf{S}_1^j] [\mathbf{S}_2^i, \mathbf{S}_2^j] \rightarrow \frac{\mathbf{S}^2}{4} \frac{2\pi C_F D_{S^2,s}^{(2)}}{d m^2} [-(d-4)(d-1)]. \tag{21}$$

For S-wave creation there is no contribution from the potentials proportional to the  $S_{12}$  and  $\mathbf{L} \cdot \mathbf{S}$  operators.

The  $D$ -dimensional prescriptions used above are irrelevant for the computation of the heavy quarkonium mass with NNLL accuracy, which reflects the fact that the leading running of the Wilson coefficients is scheme independent. On the other hand to *specify* the  $D$ -dimensional prescription of the potential is important once they are introduced into divergent potential loops. This is relevant



if we want to obtain heavy quarkonium sum rules, or to compute the  $t\bar{t}$  production near threshold with NNLL accuracy, and use computations obtained in other places for the hard matching coefficients. We would like to emphasize however that we could have chosen a different prescription. This would have changed some intermediate-step results but not the physical results.

Finally, one should note that the potential above is not equal to the potential used in Ref. [34]. Nevertheless, they can be exactly related with each other by field redefinitions (in four and  $D$  dimensions). In particular this means that the hard matching coefficients will be the same in both cases. This is actually what we expected, since they simply correspond to the effects of the (integrated out) hard modes.

The RGI coefficients of the various potentials are known to the accuracy required for evaluating the Green function at NNLL [39, 22]. Note that the strong coupling is included in the matching coefficients. Thus  $D_s^{(1)} \simeq \alpha_s^2(1 + (\alpha_s \log v)^n)$  and  $D_X^{(2)} \simeq \alpha_s(1 + (\alpha_s \log v)^n)$ . For the Coulomb potential  $\alpha_{\tilde{V}_s}$ , the exact static potential at two loop [38] receives additional three-loop LL terms proportional to  $\alpha_s^3 C_A^3 (\alpha_s \log v)^n$  [39]. The explicit form of all matching coefficients can be found in Ref. [22]. However, we have changed the basis of potentials compared to Ref. [22]. This affects the matching coefficient  $D_{d,s}^{(2)}$ , which now reads ( $\mu_{us} = \mu_s^2/\mu_h$ )

$$D_{d,s}^{(2)}(\mu_{us}) = \frac{\alpha_s(\mu_s)}{3} (2 + c_D(\mu_s)) + \frac{1}{3\pi} \left( d_{vs}(\mu_s) + \frac{1}{C_F} d_{ss}(\mu_s) \right) + \frac{32}{9\beta_0} \left( \frac{C_A}{2} - C_F \right) \alpha_s(\mu_s) \log \left[ \frac{\alpha_s(\mu_s)}{\alpha_s(\mu_{us})} \right]. \quad (22)$$

For the other potentials, the expressions obtained for their Wilson coefficients in Ref. [39, 22] hold, where one may also find the expressions for the RGI coefficients ( $c_D, d_{vs}, d_{ss}, \dots$ ) of the NRQCD operators. We repeat them in the Appendix for ease of reference.

In this paper we also include an additional contribution in  $\delta\tilde{V}$ , the electromagnetic Coulomb term

$$\delta\tilde{V} \rightarrow \delta\tilde{V} - \frac{4\pi e_Q^2 \alpha_{\text{EM}}}{\mathbf{q}^2}. \quad (23)$$

This will give rise to a NLO term  $\sim \alpha_{\text{EM}}/v$  from single potential photon exchange and a NNLO term from double potential photon exchange. Strictly speaking, the coupling in Eq. (23) should be evaluated at the soft scale and not at the hard scale, but this effect is beyond NNLL.

This completes all the corrections needed at the Lagrangian level for the computation of the imaginary part of the Green function with NNLL accuracy. What is left is to obtain the RGI expressions for  $c_s$  and  $d_s$ , where  $s = 0, 1$  labels

the spin. The matching coefficient  $c_s$  is needed at NNLL whereas  $d_s$  is only needed at LL.

## 2.2 Direct ultrasoft effects to $c_s$ and $d_s$

Most of the ultrasoft contribution to the running of  $c_s$  and  $d_s$  comes in an indirect way, through the running of the potentials in the anomalous dimensions of the RG equation. Nevertheless, there are some genuine ultrasoft effects that have not been considered so far. They are due to the appearance of some energy dependent potentials with the structure

$$\delta V_{us} = (H_c - E)Z^{1/2}, \quad (24)$$

where  $Z$  is the normalization correction to the heavy quarkonium propagator. Therefore,  $Z^{1/2}$  corresponds to the normalization of the field that represents the heavy quarkonium.  $\delta V_{us}$  was not included in Eq. (20), as there only energy independent potentials were considered. Its effects could be reabsorbed in field redefinitions of the fields that represent the heavy quarkonium. Therefore, they have no consequences in the spectrum. Nevertheless, these field redefinitions change the vertex interaction of the heavy quarkonium with photons producing changes in  $c_s$  and  $d_s$  and they have to be considered in our computation. The leading logarithmic corrections to  $Z^{1/2}$  were obtained in Eqs. (15–18) of Ref. [17] (for some partial results see also Ref. [16]). They produce corrections of order  $\alpha_s^3 \log \alpha_s$ . We can obtain the RGI expressions for them and generate terms of order  $\alpha_s^{(n+3)} \log^{(1+n)} \alpha_s$ . Note that the running goes up to the soft scale because one gets expressions of the form  $\langle \mathbf{r} = 0 | \log r | \mathbf{p} \rangle$  and the logarithm gets the scale of  $p$ . The corrections to the Green function due to Eq. (24) read

$$\delta G_1 = \frac{4\alpha_s^2}{\beta_0} \log \left[ \frac{\alpha_s(\mu_s)}{\alpha_s(\mu_{us})} \right] \frac{1}{H_c - E} \frac{C_A^2 C_F}{4}, \quad (25)$$

$$\delta G_2 = \frac{4\alpha_s}{\beta_0} \log \left[ \frac{\alpha_s(\mu_s)}{\alpha_s(\mu_{us})} \right] \left\{ \frac{1}{mr}, \frac{1}{H_c - E} \right\} \left( \frac{2}{3} C_F^2 + C_F C_A \right), \quad (26)$$

$$\delta G_3 = \frac{4}{\beta_0} \log \left[ \frac{\alpha_s(\mu_s)}{\alpha_s(\mu_{us})} \right] \left\{ \frac{\mathbf{p}^2}{m^2}, \frac{1}{H_c - E} \right\} \frac{2}{3} C_F. \quad (27)$$

The correction coming from  $\delta G_3$  can be included in  $d_s$ :

$$d_s \rightarrow d_s + \frac{16C_F}{\beta_0} \log \left[ \frac{\alpha_s(\mu_{us})}{\alpha_s(\mu_s)} \right]. \quad (28)$$

The correction from  $\delta G_2$  is zero. Finally, the correction from  $\delta G_1$  could be absorbed in  $c_s$ :

$$c_s \rightarrow c_s + \frac{\alpha_s^2 C_A^2 C_F}{2 \beta_0} \log \left[ \frac{\alpha_s(\mu_s)}{\alpha_s(\mu_{us})} \right]. \quad (29)$$

Note also that these changes are equivalent to a change in the NNLO and LO anomalous dimension of the RG equation describing the running of  $c_s$  and  $d_s$  respectively.

## 2.3 Running of $d_s$

The LL running of  $\text{Im}g_{\text{EM}}^{\text{pNR}}$  can be obtained in two steps. In the first step one computes its soft running. This has been done in Ref. [40, 41]. For the explicit result see Eqs. (C.18,C.19) in Ref. [41]. The ultrasoft running can be obtained from Eq. (28). Adding everything together the LL running of  $\text{Im}g_{\text{EM}}^{\text{pNR}}$  reads

$$\text{Im}g_{\text{EM}}^{\text{pNR}}(^1S_0)(\mu_s) = \quad (30)$$

$$\text{Im}g_{\text{EM}}^{\text{pNR}}(^1S_0)(\mu_h) - \frac{16}{3\beta_0}C_F \text{Im}f_{\text{EM}}^{\text{pNR}}(^1S_0)(\mu_h) \log \left[ \frac{\alpha_s(\mu_{us})}{\alpha_s(\mu_h)} \right],$$

$$\text{Im}g_{\text{EM}}^{\text{pNR}}(^3S_1)(\mu_s) = \quad (31)$$

$$\text{Im}g_{\text{EM}}^{\text{pNR}}(^3S_1)(\mu_h) - \frac{16}{3\beta_0}C_F \text{Im}f_{\text{EM}}^{\text{pNR}}(^3S_1)(\mu_h) \log \left[ \frac{\alpha_s(\mu_{us})}{\alpha_s(\mu_h)} \right]$$

The last result agrees with the LL result obtained in Ref. [29]. For the matching coefficient  $d_1$  as defined in Eq. (10), this entails

$$d_1(\mu_{us}) = 1 + \frac{16C_F}{\beta_0} \log \left[ \frac{\alpha_s(\mu_{us})}{\alpha_s(\mu_h)} \right]. \quad (32)$$

## 2.4 Running of $c_s$

The running of  $c_s$  is not yet known with NNLL accuracy. It is dictated by the solution of the RG equation (the LO anomalous dimension is zero)

$$\mu_s \frac{d}{d\mu_s} \log c_s = \gamma_{c_s}^{\text{NLO}} + \gamma_{c_s}^{\text{NNLO}} + \dots \quad (33)$$

The structure of the solution reads

$$c_s(\mu_s) = c_s(\mu_h) e^{\alpha_s(\mu_h)\Gamma_{c_s}^{\text{NLL}}(\mu_s) + \alpha_s^2(\mu_h)\Gamma_{c_s}^{\text{NNLL}}(\mu_s) + \dots}. \quad (34)$$

Expressions for  $c_s(\mu_h)$  at two loops in the  $\overline{\text{MS}}$  can be found in Ref. [36] for  $s = 1$  and (almost complete) in Ref. [37] for  $s = 0$ .

The expression for  $\gamma_{c_s}^{\text{NLO}}$  in the basis of potentials used in this paper reads

$$\gamma_{c_s}^{\text{NLO}} = -\frac{C_F^2}{4}\alpha_s \left[ \alpha_s + \left( 2 - \frac{4}{3}s(s+1) \right) D_{S^2,s}^{(2)} - 3D_{d,s}^{(2)} + 4D_{1,s}^{(2)} \right] - \frac{C_A C_F}{2} D_s^{(1)}. \quad (35)$$

The expression of  $\Gamma_{c_s}^{\text{NLL}}$  is known [26, 23]. For  $\Gamma_{c_s}^{\text{NNLL}}$  only the spin-dependent term is completely known [27]. Its contribution to the spin-one case reads

$$\delta\Gamma_{c_1,SD}^{\text{NNLL}}(\mu_s) = \Gamma_{\hat{c}_v}^{\text{NNLL}} + \frac{11}{72}C_F^2 \frac{\alpha_s(\mu_s)}{\alpha_s^2(\mu_h)} D_{S^2,s}^{(2)}(\mu_s) - \frac{11}{72}C_F^2, \quad (36)$$

where  $\Gamma_{\hat{c}_v}^{\text{NNLL}}$  corresponds to the result quoted in Ref. [27]. Note that we use a different expression for the spin-dependent term than just  $\Gamma_{\hat{c}_v}^{\text{NNLL}}$ . The expression above corresponds to the spin-dependent contribution to the vector current matching coefficient in the  $\overline{\text{MS}}$  scheme. Numerically this contribution is small compared with others.

Besides the spin-dependent correction, we have also incorporated the following spin-independent corrections at NNLL order (to these corrections one obviously has to subtract the spin-dependent piece that has already been included in  $\delta\Gamma_{c_1,SD}^{\text{NNLL}}$ ):

- a) those that appear from the exponentiation of the NLL term and formally are NNLL (see Eq. (34)),
- b) Effects due to the two-loop beta running of  $\alpha_s$ . They produce the following correction:

$$\begin{aligned} \alpha_s^2(\mu_h)\delta\Gamma_{c_1,b}^{\text{NNLL}}(\mu_s) &= \frac{\beta_1}{2\beta_0^2} \int_{\alpha_s(\mu_h)}^{\alpha_s(\mu_s)} \frac{d\alpha_s}{\alpha_s} \gamma_{c_s}^{\text{NLO}} \\ &\quad - \frac{2\pi}{\beta_0} \int_{\alpha_s(\mu_h)}^{\alpha_s(\mu_s)} \frac{d\alpha_s}{\alpha_s} \beta_1 \frac{\partial\alpha_s(\mu_s^2/\mu_h)}{\partial\beta_1} \frac{\partial\gamma_{c_s}^{\text{NLO}}}{\partial\alpha_s(\mu_s^2/\mu_h)}. \end{aligned} \quad (37)$$

The last term is generated from the fact that in the determination of  $\Gamma_{c_s}^{\text{NLL}}(\mu_s)$ , the relation

$$\frac{\alpha_s(\mu_s^2/\mu_h)}{\alpha_s(\mu_s)} \rightarrow \frac{1}{(2 - z^{\beta_0})}, \quad (38)$$

where  $z^{\beta_0} = \alpha_s(\mu_s)/\alpha_s(\mu_h)$ , was used. This relation is only true at one loop and has to be corrected by  $\beta_1$  terms if a NNLL accuracy is demanded. The numerical impact of these corrections is small.

- c) We have also incorporated the corrections proportional to  $a_1$ , the one-loop log-independent term, that appears in  $\alpha_{V_s} \simeq \alpha_s(\mu_s) \left(1 + \frac{\alpha_s}{4\pi} a_1\right)$ . These corrections can be deduced from the computation of the NLO anomalous dimension. They read

$$\alpha_s^2(\mu_h)\delta\Gamma_{c_1,c}^{\text{NNLL}}(\mu_s) = -\frac{1}{2\beta_0} a_1 \int_{\alpha_s(\mu_h)}^{\alpha_s(\mu_s)} \frac{d\alpha_s}{\alpha_s} \left( \gamma_{c_s}^{\text{NLO}} + \frac{C_A C_F}{2} D_s^{(1)} - C_F^2 \frac{\alpha_s^2}{4} \right). \quad (39)$$

The numerical impact of these corrections is small.

Finally, the inclusion of the electromagnetic corrections produces some corrections to  $c_1$ . Counting  $\alpha_{\text{EM}} \sim \alpha_s^2$ , the one-loop exchange of a hard photon

contributes at NNLO and is taken into account by

$$c_1(\mu_h) \rightarrow c_1(\mu_h) - \frac{2 e_Q^2 \alpha_{\text{EM}}}{\pi} \quad (40)$$

for the spin-one case, whereas for  $s = 0$  we have

$$c_0(\mu_h) \rightarrow c_0(\mu_h) - \frac{e_Q^2 \alpha_{\text{EM}}}{\pi} \left( \frac{5}{2} - \frac{\pi^2}{8} \right). \quad (41)$$

## 2.5 Green function

Once the RGI potential and current matching coefficients are available, we are in a position to use standard quantum mechanics perturbation theory to compute the higher-order corrections to  $\text{Im}[G(\mathbf{0}, \mathbf{0}; E)]$  via insertions of the potentials. This calculation has been done in momentum space using dimensional regularization. For the terms suppressed by two powers of  $\alpha_s \sim v$  in  $\delta\tilde{V}$ , Eq.(20), it is sufficient to consider a single insertion,

$$\delta G(\mathbf{0}, \mathbf{0}; E) = \int \prod_{i=1}^4 \frac{d^d \mathbf{p}_i}{(2\pi)^d} \tilde{G}_c(\mathbf{p}_1, \mathbf{p}_2; E) \delta\tilde{V}(\mathbf{p}_2, \mathbf{p}_3) \tilde{G}_c(\mathbf{p}_3, \mathbf{p}_4; E), \quad (42)$$

whereas for terms suppressed by only a single power of  $\alpha_s \sim v$  we have to compute double insertions as well,

$$\delta G(\mathbf{0}, \mathbf{0}; E) = \int \prod_{i=1}^6 \frac{d^d \mathbf{p}_i}{(2\pi)^d} \tilde{G}_c(\mathbf{p}_1, \mathbf{p}_2; E) \delta\tilde{V}(\mathbf{p}_2, \mathbf{p}_3) \tilde{G}_c(\mathbf{p}_3, \mathbf{p}_4; E) \delta\tilde{V}(\mathbf{p}_4, \mathbf{p}_5) \tilde{G}_c(\mathbf{p}_5, \mathbf{p}_6; E). \quad (43)$$

Since the RGI does not alter the structure of the interaction terms, the insertions can be taken directly from Ref. [34]. In Appendix A we list the integrals that are needed and present the explicit results obtained in Ref. [34].

In the calculation described so far, the on-shell scheme for the heavy quark mass has been implicitly assumed. In order to avoid the bad convergence behaviour inherent to this scheme, it is necessary to rewrite the expressions in terms of a threshold mass which is free of the renormalon ambiguity. In this paper we will consider the cases of the potential subtracted (PS) mass [32] and renormalon subtracted (RS) mass [33]. We will use the difference between both schemes as an indication of the scheme dependence of our results.

## 3 The case of the top quark

In this section we apply the previous results to the case of top-quark pair production near threshold at a future linear collider. Due to the large width  $\Gamma_t$  of the

top quark there are no bound states and the toponium resonances are smeared, resulting in a smooth curve for the cross section with a broad peak as the remnant of the would-be  $1S$  bound state. Using perturbation theory we can reliably compute the cross section as a function of the energy [1]. This may lead to accurate determinations of the top mass and its total decay width by measuring the position and normalization of the peak.

The  $t\bar{t}$  pair will be dominantly produced via  $e^+e^- \rightarrow \gamma^*, Z^* \rightarrow t\bar{t}$ . The total production cross section may be written as [3]

$$\sigma_{\text{tot}}^{\gamma,Z}(s) = \frac{4\pi\alpha_{\text{EM}}^2}{3s} \left[ F^v(s) R^v(s) + F^a(s) R^a(s) \right], \quad (44)$$

where

$$\begin{aligned} R^v(s) &= \frac{4\pi}{s} \text{Im} \left( -i \int d^4x e^{iq \cdot x} \langle 0 | T \{ j_\mu^v(x) j^{v\mu}(0) \} | 0 \rangle \right), \\ R^a(s) &= \frac{4\pi}{s} \text{Im} \left( -i \int d^4x e^{iq \cdot x} \langle 0 | T \{ j_\mu^a(x) j^{a\mu}(0) \} | 0 \rangle \right), \end{aligned} \quad (45)$$

and  $j_\mu^v$  ( $j_\mu^a$ ) is the vector (axial-vector) current that produces a quark-antiquark pair defined by Eq. (10). With both  $\gamma$  and  $Z$  exchange the prefactors in Eq. (44) are

$$\begin{aligned} F^v(s) &= \left[ e_q^2 - \frac{2s v_e v_q e_q}{s - m_Z^2} + \frac{s^2 (v_e^2 + a_e^2) v_q^2}{(s - m_Z^2)^2} \right], \\ F^a(s) &= \frac{s^2 (v_e^2 + a_e^2) a_q^2}{(s - m_Z^2)^2}, \end{aligned} \quad (46)$$

where

$$v_f = \frac{T_3^f - 2e_f \sin^2 \theta_W}{2 \sin \theta_W \cos \theta_W}, \quad a_f = \frac{T_3^f}{2 \sin \theta_W \cos \theta_W}. \quad (47)$$

Here  $e_f$  is the charge for fermion  $f$ ,  $T_3^f$  is the third component of weak isospin,  $\theta_W$  is the weak mixing angle, and  $m_Z$  the mass of the  $Z$ . Here we will focus on  $R^v$ , since it gives the dominant contribution and we are mainly interested in studying the impact of the resummation of logarithms on the convergence and scale dependence of the perturbative expansion of  $R^v$ . A study of  $R^a$  can be found in Ref. [29].

Since  $\Gamma_t \sim m\alpha_{\text{EM}} \sim mv^2$  and the propagator of a potential heavy quark scales as  $v^{-2}$  the effects due to the width of the top quark are LO effects and have to be taken into account by modifying the propagator  $E - \mathbf{p}^2/(2m) \rightarrow E + i\Gamma_t - \mathbf{p}^2/(2m)$ . This amounts to replacing  $E \rightarrow E + i\Gamma_t$  in Eq. (1). As noted in Ref. [1], this is only correct at LO. Higher-order electroweak corrections have a much richer structure and it is not possible any longer to formulate the problem

in terms of a  $t\bar{t}$  final state. In particular, at NNLO there are interference effects (between double and single resonant processes), QED radiation effects and non-factorizable corrections (non-trivial interconnections between the decay products of the top quarks with the remainder of the process). Any consistent approach beyond LO has to introduce additional operators with fields corresponding to the incoming electrons and the decay products of the top quarks, and link higher-order corrections of the  $\psi^\dagger\psi$  and  $\chi^\dagger\chi$  operators to three-point and higher-point vertices. Even though there is an effective theory framework available for systematically taking into account these corrections [42], a full explicit calculation of electroweak effects at NNLO is still lacking. If we are interested in the total cross section only, the situation is somewhat simpler, since the non-factorizable corrections cancel [43], and the replacement  $E \rightarrow E + i\Gamma_t$  becomes correct with NLO accuracy. Furthermore, some of the electroweak corrections have been taken into account by including them in the matching coefficients [44]. In this article we restrict ourselves to the usual shift  $E \rightarrow E + i\Gamma_t$ .

In Figure 1 the fixed-order results are compared to the RGI results obtained using the procedure described above and using the PS mass with the subtraction scale  $\mu_F$  required for the definition of the threshold mass set to 20 GeV. The plots were produced with an energy dependent soft scale  $\mu_s^2 = 4m\sqrt{E^2 + \Gamma_t^2}$ . In order to obtain a first rough estimate of the theoretical uncertainty we show the cross sections as bands obtained by variation of the soft scale in the region  $30 \text{ GeV} \leq \mu_s \leq 80 \text{ GeV}$ , where these numbers refer to the scale  $\mu_s$  at  $E = 0$ . For the hard and ultrasoft scale we take our default values  $\mu_h = m_{\text{PS}} = 175 \text{ GeV}$  and  $\mu_{us} = \mu_s^2/\mu_h$ . Our results are qualitatively consistent, but not equal, to those obtained in Refs. [28, 29]. This agreement is not trivial, since the ingredients included in the NNLL analysis are different in ours and their computations. This may indicate that, even if the NNLL evaluation is incomplete, the qualitative features will hold in the complete result. We observe that the scale dependence is much reduced once the logarithms are taken into account and reduces from LL to NLL to NNLL. We also note that the size of the corrections decreases for the RGI results, in particular the NNLL band is much closer to the NLL band. However, the NNLL band does not overlap with the NLL band, indicating that a theoretical error estimate relying on the scale dependence alone is too optimistic. Therefore, we consider other possible source of errors in what follows.

The variation of the soft scale has been stopped at  $\mu_s = 30 \text{ GeV}$  which might seem to be a rather large value. In fact, the dependence of the normalization of the peak as a function of  $\mu_s$  is very smooth at NNLL, up to a value of  $\mu_s \sim 25 \text{ GeV}$ , where it abruptly changes<sup>2</sup>. At NLL, already for  $\mu_s \sim 30 \text{ GeV}$  there is a rather large variation of the normalization. This is illustrated in Figure 2 which shows the  $\mu_s$  dependence of the normalization of the peak at LO/LL, NLO, NLL, NNLO

---

<sup>2</sup>As we will see a similar pattern also appears for the bottomonium decays.

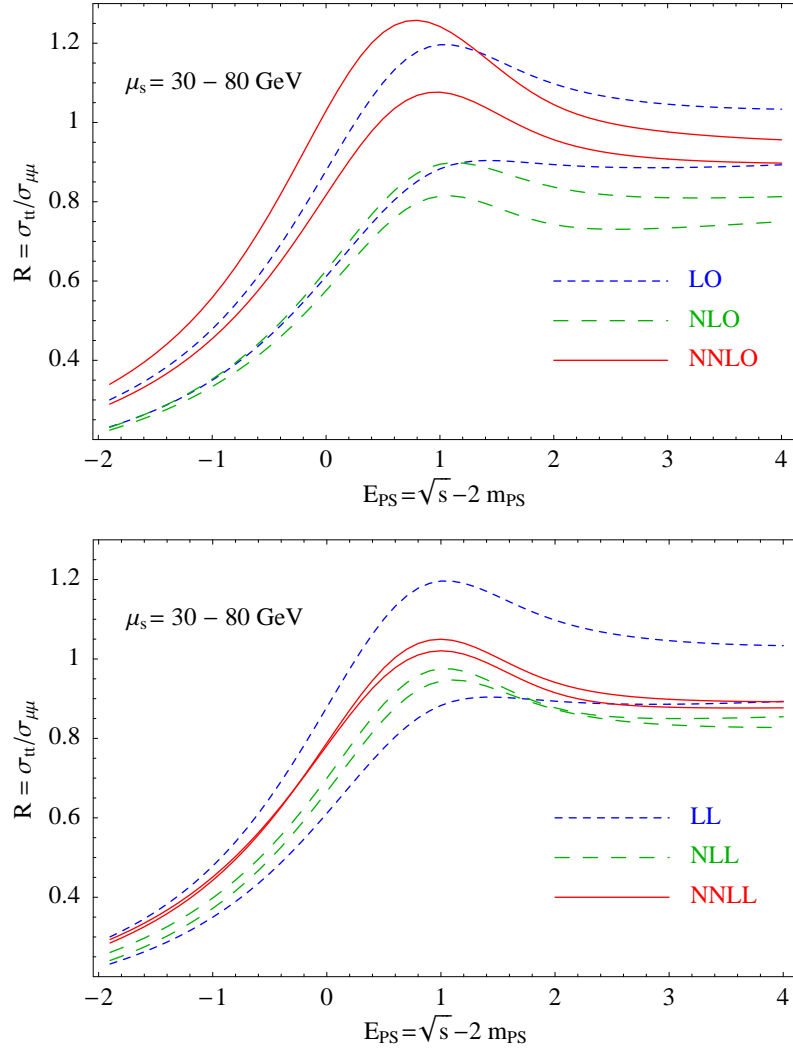


Figure 1: Threshold scan for  $t\bar{t}$  using the PS mass,  $m_{\text{PS}}(20 \text{ GeV}) = 175 \text{ GeV}$ . The upper panel shows the fixed order results, LO, NLO and NNLO, whereas in the lower panel the RGI results LL, NLL and NNLL are displayed. The soft scale is varied from  $\mu_s=30 \text{ GeV}$  to  $\mu_s=80 \text{ GeV}$ .

and NNLL. As observed in Ref. [20] the situation for small soft scales may be remedied if multiple insertions of the Coulomb potential are taken into account. Since in our result these, formally, higher-order contributions are not taken into account, we refrain from using scales  $\mu_s \leq 30 \text{ GeV}$  and take  $\mu_s = 40 \text{ GeV}$  as our default value for the soft scale unless stated otherwise. The “NNNLO” result also depicted in Figure 2 is obtained by re-expanding the full RGI result and keeping only terms that are NNNLO, but dropping those of even higher order. The difference between this result and the full RGI result is small except for scales  $\mu_s \leq 30 \text{ GeV}$ , which is outside the range we use.



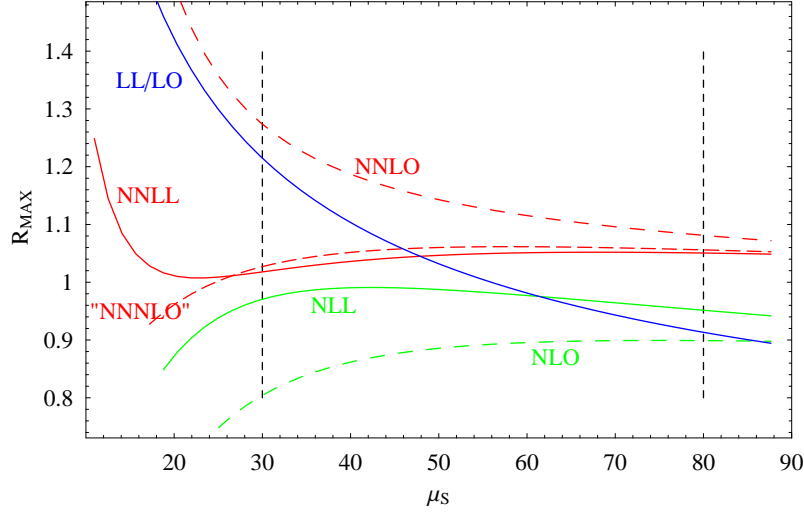


Figure 2: The normalization of the peak of the RGI threshold cross section as a function of the soft scale  $\mu_s$ . The vertical dashed lines show the limits of variation used in Figure 1.

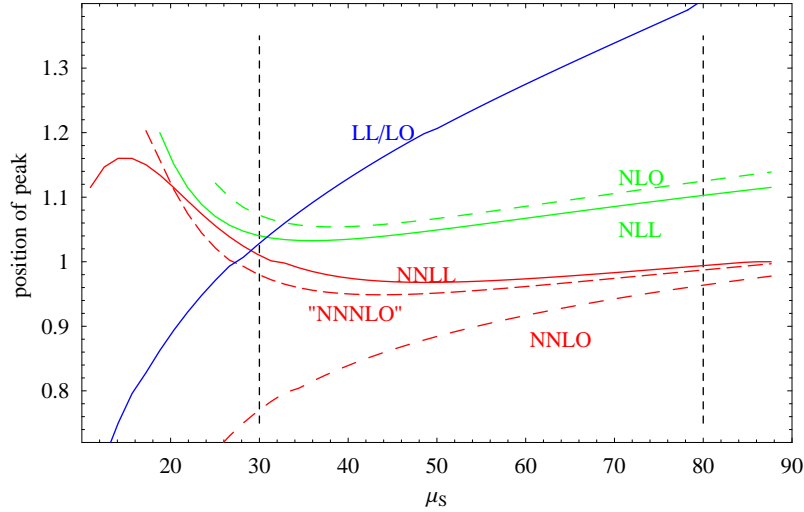


Figure 3: The position of the peak of the RGI threshold cross section as a function of the soft scale  $\mu_s$ . The vertical dashed lines show the limits of variation used in Figure 1.

We also present a similar plot to show the scale dependence of the position of the peak in Figure 3. From this plot we can see that the NNLL resummation of logarithms significantly improves over the fixed-order NNLO evaluation. The scale dependence is reduced and also the convergence of the perturbative series is better, which is reflected in a smaller difference between the NLL and NNLL

result versus the NLO and NNLO result (this also happens for the normalization of the total cross section). The difference between the “NNNLO” and NNLL curve is again very small for  $\mu_s \geq 30$  GeV. From this plot we estimate the theoretical error for the determination of the position of the peak (which is related to the determination of the top mass) to be of the order of 100 MeV.

In the fixed-order calculations the error is usually estimated from the soft-scale dependence, even though one may think that the dominant uncertainty came from the magnitude of the correction. This is potentially more of a problem after the resummation of logarithms, since the soft scale dependence is much less severe. Therefore, we have to be more careful with other sources of uncertainties. In particular, the missing ultrasoft contributions make it important to consider the dependence on the other scales as well. Since they are correlated, we can only vary  $\mu_h$  together with  $\mu_{us}$  and, thus, consider in Figure 4 the dependence on the hard scale  $\mu_h$ , setting  $\mu_s = 40$  GeV. Variation of the hard scale around its natural value  $\mu_h = m$  by choosing  $100 \text{ GeV} \leq \mu_h \leq 250 \text{ GeV}$  results in a scale dependence that is considerably larger than the soft scale dependence. We note that this error is compatible with the magnitude of the difference between the NLL and NNLL result. It is to be expected that the situation improves once all ultrasoft logarithms at NNLL are taken into account, but at this stage the rather large dependence of the cross section on  $\mu_h$  has to be taken into account if a theoretical error is assigned. We also note that the dependence on  $\mu_h$  only enters at NLL, thus the LL “band” in Figure 4 is simply a line.

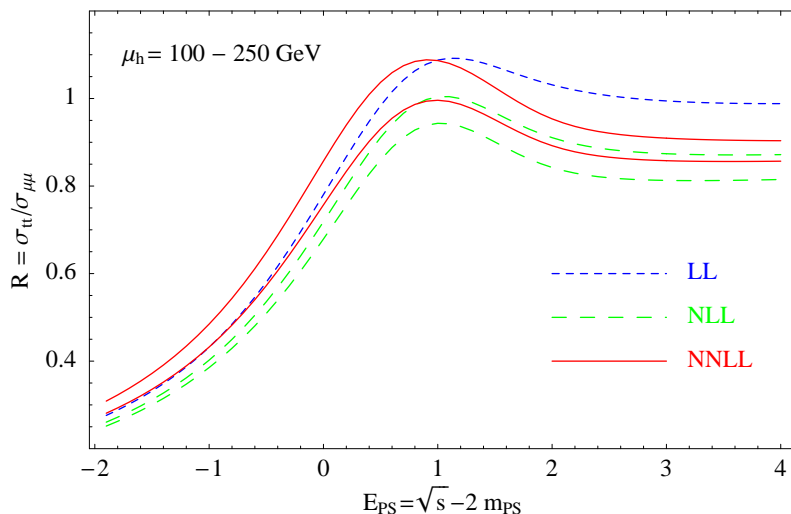


Figure 4: Dependence of the  $t\bar{t}$  threshold scan on the hard scale  $\mu_h$ , using the PS mass. At NNLL (NLL) the lower (upper) curve corresponds to  $\mu_h = 250$  GeV, whereas the upper (lower) curve corresponds to  $\mu_h = 100$  GeV.

Finally we turn to Figure 5, where we display the effects due to the QED

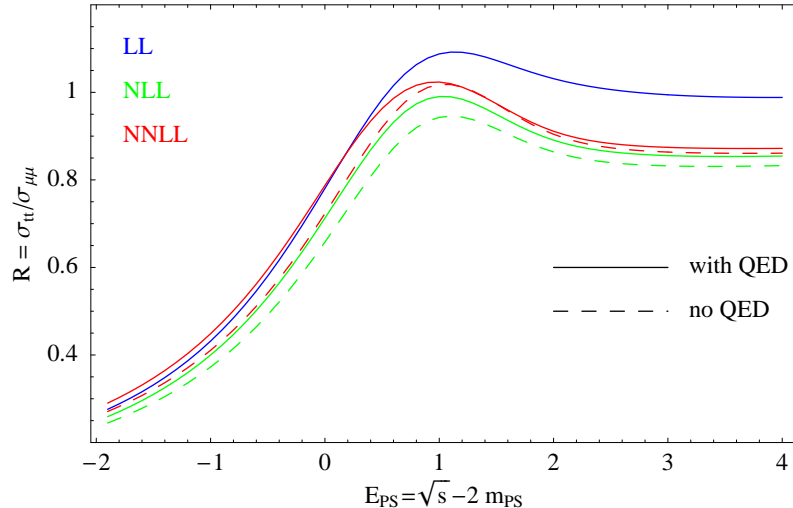


Figure 5: Effects of the QED corrections to the  $t\bar{t}$  threshold scan. The hard and soft scales are chosen as  $\mu_h = m_{\text{PS}} = 175$  GeV and  $\mu_s = 40$  GeV.

corrections with the default choice for the scales,  $\mu_h = m$  and  $\mu_s = 40$  GeV. As previously mentioned, the QED effects enter at NLL (thus there is no effect on the LL curve) and, compared to the desired accuracy (top quark mass measurement with an error  $\delta m \leq 100$  MeV), they are large. They change the normalization by up to 10% and result in a shift in the extracted  $\overline{\text{MS}}$  mass of up to 100 MeV, making it mandatory to include them. We note that we have not changed the definition of the PS mass. Thus the shifts shown in Figure 5 are physical effects and are not compensated if the PS mass is related to the  $\overline{\text{MS}}$  mass.

We end this section by mentioning that all results presented here can be worked out in different threshold mass schemes. The qualitative features of the results obtained are similar. We illustrate this point using the RS and RS' mass, again setting  $\mu_F = 20$  GeV, and depict the threshold scan in Figure 6. Those plots, together with the plot in the PS scheme (lower panel in Figure 1), allow us to visualize the effect of using different threshold masses. In principle, the value of the threshold masses can run from being numerically close to the  $\overline{\text{MS}}$  mass (but not too close otherwise power counting is broken) to being numerically close to the pole mass (but again not too close, otherwise the renormalon cancellation does not take place). Within this allowed range, the threshold mass definitions numerically closer to the  $\overline{\text{MS}}$  mass have a smaller scale dependence. The price paid is that the magnitude of the corrections (between different order in perturbation theory) is larger. For the specific threshold masses we use, the RS mass is the one closest to the  $\overline{\text{MS}}$  mass whereas the RS' mass is closest to the pole mass. The PS mass is in the middle, though somewhat closer to the RS mass. Once experimental data is available it will be useful to consider different mass definitions to obtain

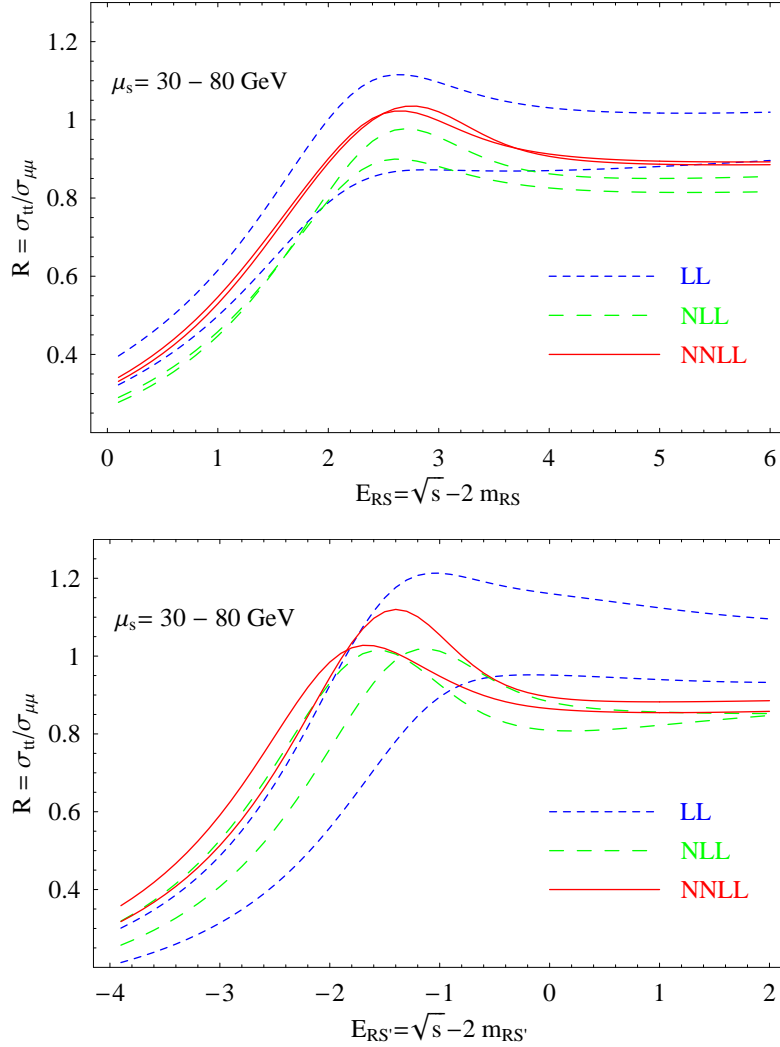


Figure 6: Threshold scan for  $t\bar{t}$  using the RS and RS' mass,  $m_{RS}(20 \text{ GeV}) = 175 \text{ GeV}$ ,  $m_{RS'}(20 \text{ GeV}) = 175 \text{ GeV}$ . The upper panel shows the RGI results LL, NLL and NNLL with the RS and the lower panel with the RS' mass. The soft scale is varied from  $\mu_s=30 \text{ GeV}$  to  $\mu_s=80 \text{ GeV}$ .

an estimate of the corresponding error.

## 4 The case of the bottom quark

We can also apply the results of Section 2 to a variety of observables for  $b\bar{b}$  systems. Likely, the theoretically cleanest observable on which one can use our results is non-relativistic sum rules, which has already been considered in Ref. [9], where an

accurate determination of the bottom mass was obtained. Here we will consider inclusive electromagnetic decays (either to  $e^+e^-$  or to  $\gamma\gamma$ ) of the bottomonium ground state for which we will provide analytic formulae. These can be obtained from the results obtained for the non-relativistic Green function. The spin-one decay has the following structure

$$\Gamma(\Upsilon(nS) \rightarrow e^+e^-) = \tag{48}$$

$$16\pi \frac{C_A}{3} \left[ \frac{\alpha_{EM} e_Q}{M_{\Upsilon(nS)}} \right]^2 |\phi_n^{(s=1)}(\mathbf{0})|^2 \left\{ c_1 - d_1 \frac{M_{\Upsilon(nS)} - 2m}{6m} \right\}^2 .$$

The corrections to the wave function at the origin are obtained by taking the residue of the Green function at the position of the poles

$$|\phi_n^{(s=1)}(\mathbf{0})|^2 = |\phi_n^{(0)}(\mathbf{0})|^2 \left( 1 + \delta\phi_n^{(s=1)} \right) = \underset{E=E_n}{\text{Res}} G_{s=1}(\mathbf{0}, \mathbf{0}; E), \tag{49}$$

where the LO wave function is given by

$$|\phi_n^{(0)}(\mathbf{0})|^2 = \frac{1}{\pi} \left( \frac{mC_F\alpha_s}{2n} \right)^3 . \tag{50}$$

The corrections to  $\delta\phi_n^{(s=1)}$  produced by  $\delta V$  have already been calculated with NNLO accuracy [5, 6] in the direct matching scheme. One can also obtain them in the dimensional regularized  $\overline{\text{MS}}$  scheme with NNLL accuracy by incorporating the RGI matching coefficients. One obtains then the following correction to the wave function

$$\begin{aligned} \delta\phi_n^{(s=1)} &= \frac{\alpha_s^2 C_A^3}{2\beta_0} \log \left[ \frac{\alpha_s(\mu_s)}{\alpha_s(\mu_{us})} \right] \tag{51} \\ &+ \frac{\alpha_s}{\pi} \left( \frac{3a_1}{4} + \frac{\beta_0}{2} \left( 3L[n] + S[1, n] + 2nS[2, n] - 1 - \frac{n\pi^2}{3} \right) \right) \\ &+ C_F C_A D_s^{(1)} \left( L[n] - S[1, n] + \frac{2}{n} + \frac{5}{4} \right) \\ &+ 2C_F^2 \alpha_s D_{1,s}^{(2)} \left( L[n] - S[1, n] - \frac{5}{8n^2} + \frac{2}{n} + \frac{3}{2} \right) \\ &- \frac{C_F^2 \alpha_s D_{S^2,s}^{(2)}}{3} \left( L[n] - S[1, n] + \frac{2}{n} + \frac{11}{12} \right) \\ &- \frac{3C_F^2 \alpha_s D_{d,s}^{(2)}}{2} \left( L[n] - S[1, n] + \frac{2}{n} + \frac{1}{2} \right) \\ &- \frac{C_F^2}{4} D_{2,s}^{(2)} \alpha_s \\ &+ c_4 \frac{C_F^2 \alpha_s^2}{2} \left( L[n] - S[1, n] - \frac{3}{4n^2} + \frac{2}{n} + \frac{3}{2} \right) \end{aligned}$$

$$\begin{aligned}
& + \frac{\alpha_s^2}{(4\pi)^2} \left( 3a_1^2 + 3a_2 - 14a_1\beta_0 + 4\beta_0^2 - 2\beta_1 + \beta_0^2\pi^2 \right. \\
& - \frac{8a_1\beta_0n\pi^2}{3} + \frac{4\beta_0^2n\pi^2}{3} - \frac{2\beta_1n\pi^2}{3} + \frac{\beta_0^2n^2\pi^4}{9} + 24a_1\beta_0L[n] \\
& - 28\beta_0^2L[n] + 6\beta_1L[n] - \frac{16\beta_0^2n\pi^2}{3}L[n] + 24\beta_0^2L[n]^2 \\
& + 8a_1\beta_0S[1, n] - 20\beta_0^2S[1, n] + 2\beta_1S[1, n] - \frac{12\beta_0^2S[1, n]}{n} - \frac{8\beta_0^2n\pi^2S[1, n]}{3} \\
& + 16\beta_0^2L[n]S[1, n] + 8\beta_0^2S[1, n]^2 + 8\beta_0^2S[2, n] + 16a_1\beta_0nS[2, n] \\
& - 8\beta_0^2nS[2, n] + 4\beta_1nS[2, n] - \frac{4\beta_0^2n^2\pi^2S[2, n]}{3} + 32\beta_0^2nL[n]S[2, n] \\
& + 16\beta_0^2nS[1, n]S[2, n] + 4\beta_0^2n^2S[2, n]^2 + 28\beta_0^2nS[3, n] - 20\beta_0^2n^2S[4, n] \\
& \left. - 24\beta_0^2nS_2[2, 1, n] + 16\beta_0^2n^2S_2[3, 1, n] + 20\beta_0^2n\zeta(3) \right),
\end{aligned}$$

where

$$L[n] = \log \left[ \frac{\mu_s n}{m C_F \alpha_s} \right], \quad S[a, n] = \sum_{k=1}^n \frac{1}{k^a}, \quad S_2[a, b, n] = \sum_{k=1}^n \frac{1}{k^a} S[b, k]. \quad (52)$$

For completeness we also give the corrections to the wave function induced by the QED effect, Eq. (23). They read

$$\begin{aligned}
\delta\phi_n^{(s=1)} \rightarrow \delta\phi_n^{(s=1)} & + \frac{3e_Q^2\alpha_{EM}}{C_F\alpha_s} + \frac{e_Q^2\alpha_{EM}}{C_F\pi} \left( \frac{3a_1}{2} + \frac{3\pi e_Q^2\alpha_{EM}}{C_F\alpha_s^2} \right. \\
& \left. + \beta_0 \left( 3L[n] + S[1, n] + 2nS[2, n] - \frac{5}{2} - \frac{n\pi^2}{3} \right) \right). \quad (53)
\end{aligned}$$

Of course, the corrections to the matching coefficients of the current, Eqs. (40) and (41) have to be taken into account as well. Due to the additional suppression  $e_Q^2 = 1/9$  these QED corrections are numerically not very important.

From these expressions one can obtain the wave-function correction for the spin zero case

$$\delta\phi_n^{(s=0)} = \delta\phi_n^{(s=1)} + \delta\phi_n^{\Delta s}, \quad (54)$$

where

$$\delta\phi_n^{\Delta s} = -\frac{2}{3}C_F^2 D_{S^2, s}^{(2)} \alpha_s \left( -2L[n] + 2S[1, n] - \frac{4}{n} - \frac{7}{3} \right) \quad (55)$$

by using the results from Ref. [27]. Therefore, the decay of the pseudoscalar heavy quarkonium to two photons reads ( $d_0 = d_1$ )

$$\begin{aligned}
\Gamma(\eta_b(nS) \rightarrow \gamma\gamma) & = \quad (56) \\
16\pi C_A \left[ \frac{\alpha_{EM} e_Q^2}{M_{\eta_b(nS)}} \right]^2 & \left| \phi_n^{(s=0)}(\mathbf{0}) \right|^2 \left\{ c_0 - d_0 \frac{M_{\eta_b(nS)} - 2m}{6m} \right\}^2.
\end{aligned}$$

We now perform a phenomenological analysis of these results. We restrict our analysis to the ground state of bottomonium. For the mass of the  $\eta_b(1S)$ , we use the  $\Upsilon(1S)$  mass, which is consistent to the order of interest. When we perform the numerical analysis, we expand the expressions (except for the overall factor  $1/M_{\Upsilon(1S)/\eta_b(1S)}^2$ ) in Eqs. (48) and (56), and drop subleading corrections, in order to work strictly at LL, NLL (NLO) and NNLL (NNLO). In particular, this applies to the relativistic correction proportional to  $d_s$ , where  $M_{\Upsilon(1S)/\eta_b(1S)} - 2m$  is replaced by  $E_1^{(0)} = -mC_F^2\alpha_s^2/4$ . The expressions above have been written in the pole scheme. Therefore, we change to a threshold scheme suitable for the renormalon cancellation. We consider three possible schemes: the PS, the RS and the RS' scheme with the subtraction scale  $\mu_F = 2$  GeV. The numerical values of the bottom-quark mass to be used in the various schemes are taken from Ref. [9] and are given by  $m_{\text{PS}}(2 \text{ GeV}) = 4.515$  GeV,  $m_{\text{RS}}(2 \text{ GeV}) = 4.370$  GeV, and  $m_{\text{RS}'}(2 \text{ GeV}) = 4.750$  GeV. Apart from the different numerical values for  $m$  to be used, the first change in the formulae appears (at most) at NNLL (NNLO) and is due to the shift

$$m \rightarrow m_X(\mu_f) + \delta m_X(\mu_f) \quad (57)$$

$$\Gamma|_m \rightarrow \Gamma|_{m \rightarrow m_X} + 3 \frac{\delta m_X}{m_X} \Gamma^{(0)}, \quad (58)$$

where  $m_X$  represents a generic threshold mass,  $\Gamma^{(0)}$  is the decay width at lowest order and the shift in the mass  $\delta m_X \sim mv^2$ . We notice that in the RS' scheme  $\delta m_{\text{RS}'} = 0$  at order  $mv^2$ . Therefore, in this scheme, with the current precision of the calculation, the expressions for  $\Gamma$  are equivalent to those in the pole mass scheme.

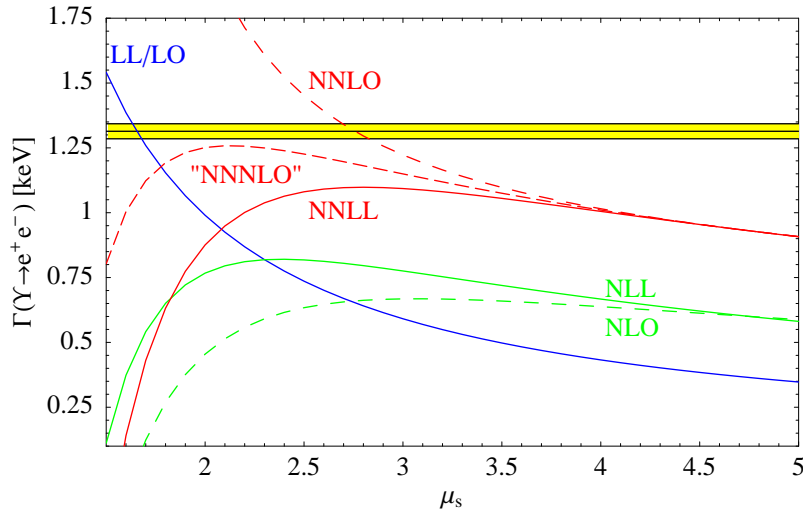


Figure 7: Prediction for the  $\Upsilon(1S)$  decay rate to  $e^+e^-$ . We work in the RS' scheme.

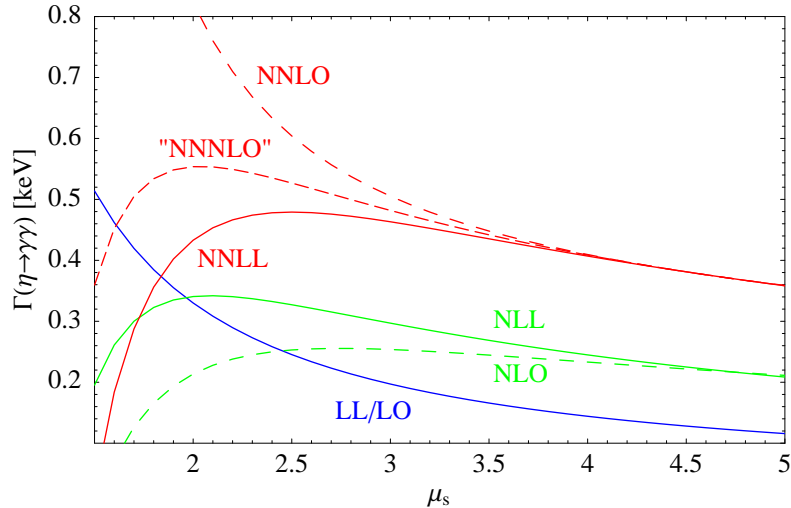


Figure 8: Prediction for the  $\eta_b(1S)$  decay rate to two photons. We work in the RS' scheme.

The results for the vector and pseudoscalar decay can be found in Figure 7 and Figure 8 respectively. From the numerical analysis, we find that the NNLL corrections are huge, especially for the  $\eta_b(1S) \rightarrow \gamma\gamma$  decay. The result we obtain for this decay is compatible with the number obtained in Ref. [27]. This is somewhat reassuring, since in that reference the ratio of the spin-one spin-zero decay was considered, which was much more scale independent, as well as more convergent (yet still large) than for each of the decays themselves. This agreement can be traced back to the fact that, for the spin-one decay, for which we can compare with experiment, we find that the NNLL result improves the agreement with the data. Overall, the resummation of logarithms always significantly improves over the NNLO result, the scale dependence greatly improves, as well as the convergence of the series. On the other hand the problem of lack of convergence of the perturbative series is not really solved by the resummation of logarithms and it remains as an open issue. Due to the lack of convergence we refrain from giving numbers (and assigning errors) for our analysis. In this respect we can not avoid to mention that, whereas the perturbative series in non-relativistic sum rules is sign-alternating, is not sign-alternating for the electromagnetic decays. Finally, we would also like to remark the strong scale dependence that we observe at low scales, which we believe to have the same origin than the one observed in  $t\bar{t}$  production near threshold in the previous section.

As for the  $t\bar{t}$  case the “NNNLO” curve, which contains the logarithmically enhanced NNNLO terms, follows closely the RGI curve up to a certain value of  $\mu_s$ . For smaller soft scales, the two curves start to deviate. However, in the  $b\bar{b}$  case, this deviation takes place already for reasonably large values of  $\mu_s \sim 2.5$  GeV.



This seems to suggest that resummation is rather more important in the  $b\bar{b}$  case. However, we have to keep in mind that some logarithms at NNLL are still missing in our analysis and this might well affect this conclusion.

We also illustrate the dependence on the threshold mass evaluation in Figure 9. Compared with the uncertainty due to the lack of convergence of the perturbative series, the dependence on the threshold mass is negligible.

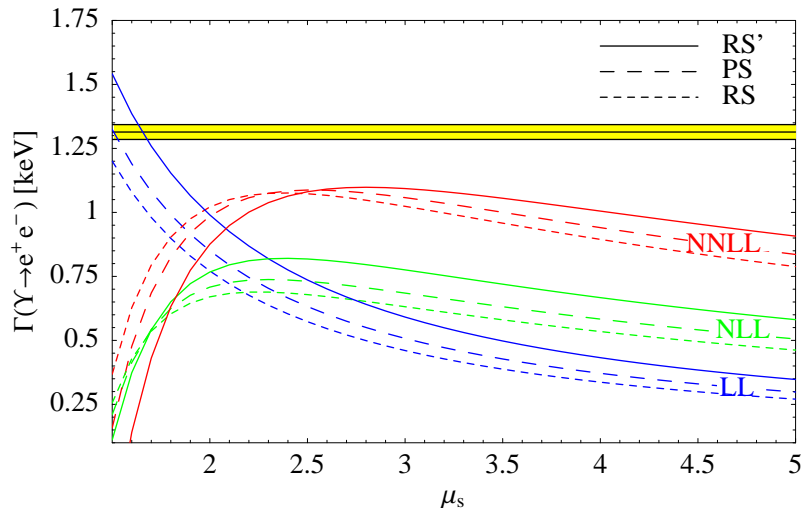


Figure 9: Prediction for the  $\Upsilon(1S)$  decay rate to  $e^+e^-$  at LL, NLL and NNLL for the PS, RS and RS' mass.

## 5 Conclusions

We have studied the effect of the resummation of logarithms for  $t\bar{t}$  production near threshold and inclusive electromagnetic decays of heavy quarkonium. This analysis is complete at NNLO and includes the full resummation of logarithms at NLL accuracy and some partial contributions at NNLL accuracy.

Compared with fixed-order computations the scale dependence and convergence of the perturbative series is greatly improved for both the position of the peak and the normalization of the total cross section of  $t\bar{t}$  production near threshold. Nevertheless, we identify a possible source of a large scale dependence in the result. While the result is very stable with respect to the variation of the soft scale  $\mu_s$  it shows a considerably larger dependence on the hard scale  $\mu_h$ . This might well be related to the fact that the variation with respect to  $\mu_h$  is correlated with the ultrasoft scale variation and the ultrasoft logarithms are not fully included at the NNLL level in our result. At present we estimate the remaining

theoretical uncertainty of the normalization of the total cross section to be of the order of 10% and for the position of the peak of the order of 100 MeV, based on the difference between the NLL and NNLL plots, as well as on the hard scale dependence. We note that this estimate of the theoretical error is somewhat larger than in Ref. [45], due to the fact that we use more possible sources of the theoretical error. We would like to remark that the use of the RGI provides us also with a significantly improved determination of the top mass.

For the inclusive electromagnetic bottomonium decays the corrections are even larger than in the top case. In the case of the  $\Upsilon(1S) \rightarrow e^+e^-$ , they bring the final prediction into better agreement with experiment. For the  $\eta_b \rightarrow \gamma\gamma$ , there is no experimental data at present and the presence of huge corrections make a reliable theoretical prediction difficult.

Finally we remark that the NNNLO part of the RGI results is numerically considerably more important than the even higher-order terms, in particular for the top case. Thus it would be highly desirable to combine a full NNNLO evaluation with a complete NNLL result in order to obtain a satisfactory theoretical prediction of heavy-quark pair production near threshold.

### Acknowledgments:

The work of A.P. was supported in part by a *Distinció* from the *Generalitat de Catalunya*, as well as by the contracts MEC FPA2004-04582-C02-01, CIRIT 2005SGR-00564 and the EU network EURIDICE, HPRN-CT2002-00311. A.P. acknowledges discussions with A.A. Penin and J. Soto.

## A Insertions

In this appendix we discuss how to obtain the perturbative expansion of the Green function. For the loop integration measure we use

$$\int d\tilde{p}_i \equiv \left( \frac{\mu^2 e^{\gamma_E}}{4\pi} \right)^\epsilon \int \frac{d^d \mathbf{p}_i}{(2\pi)^d} \quad (59)$$

such that the  $\overline{\text{MS}}$ -scheme corresponds to minimally subtracting the poles in  $\epsilon$ . We start by writing the potential, Eq. (20), for the case of a spin triplet S wave

$$\begin{aligned} \delta\tilde{V}\Big|_{3S_1} &= -\frac{C_F\alpha_s^2}{\mathbf{q}^2} \left( a_1 - \beta_0 \log \frac{\mathbf{q}^2}{\mu_s^2} \right) - \frac{C_F\alpha_s^3}{\mathbf{q}^2} \frac{C_A^3}{6\beta_0} \log \left[ \frac{\alpha_s(\mu_s)}{\alpha_s(\mu_{us})} \right] \\ &\quad - c_4 \frac{p^4}{4m^3} (2\pi)^d \delta^{(d)}(\mathbf{q}) - \frac{2\pi C_F D_{1,s}^{(2)}}{m^2} \frac{\mathbf{p}^2 + \mathbf{p}'^2}{\mathbf{q}^2} \\ &\quad - \frac{C_F\alpha_s^3}{4\pi \mathbf{q}^2} \left( a_2 - (2a_1\beta_0 + \beta_1) \log \frac{\mathbf{q}^2}{\mu_s^2} + \beta_0^2 \log^2 \frac{\mathbf{q}^2}{\mu_s^2} \right) \end{aligned} \quad (60)$$

$$\begin{aligned}
& + \frac{3\pi C_F D_{d,s}^{(2)}}{m^2} - \frac{\pi C_F D_{S^2,s}^{(2)}}{m^2} \frac{(d-4)(d-1)}{d} \\
& - \frac{\pi^2 C_F C_A D_s^{(1)}}{m q^{1+2\epsilon}} (1-\epsilon) \frac{e^{\epsilon\gamma_E}}{\mu_s^{-2\epsilon}} \frac{\Gamma^2(\frac{1}{2}-\epsilon)\Gamma(\frac{1}{2}+\epsilon)}{\pi^{3/2}\Gamma(1-2\epsilon)} \\
& + \frac{\pi C_F D_{2,s}^{(2)}}{m^2} \left( \left( \frac{\mathbf{p}^2 - \mathbf{p}'^2}{\mathbf{q}^2} \right)^2 - 1 \right),
\end{aligned}$$

where we have used the explicit expression for  $\alpha_{\tilde{V}_s}$ . The terms in the first line of Eq. (60) are NLO and we have to consider double insertions of such terms. All other terms are NNLO. Insertions of the potentials with  $D_{d,s}^{(2)}$ ,  $D_{S^2,s}^{(2)}$ ,  $D_s^{(1)}$  and  $D_{2,s}^{(2)}$  result in divergences. Thus, the corresponding coefficients have to be known in  $d$  dimensions. The insertions with  $c_4$ ,  $D_{1,s}^{(2)}$  and  $D_{2,s}^{(2)}$  can be related to other insertions, discussed below, using the  $d$ -dimensional equation

$$\begin{aligned}
\left( \frac{\mathbf{p}^2}{m} - E \right) \tilde{G}_c(\mathbf{p}, \mathbf{p}'; E) &= \tag{61} \\
(2\pi)^d \delta^{(d)}(\mathbf{p} - \mathbf{p}') + \int \frac{d^d \mathbf{k}}{(2\pi)^d} \frac{4\pi C_F \alpha_s}{\mathbf{k}^2} \tilde{G}_c(\mathbf{p} - \mathbf{k}, \mathbf{p}'; E).
\end{aligned}$$

For the terms in the second line of Eq. (60) we get

$$\begin{aligned}
\int \prod d\tilde{p}_i \tilde{G}_c(\mathbf{p}_1, \mathbf{p}_2) \left( \frac{\mathbf{p}_3^4 c_4}{4m^3} (2\pi)^d \delta^{(d)}(\mathbf{q}_{23}) + \frac{2\pi C_F D_{1,s}^{(2)}}{m^2} \frac{\mathbf{p}_2^2 + \mathbf{p}_3^2}{q_{23}^2} \right) \tilde{G}_c(\mathbf{p}_3, \mathbf{p}_4) \tag{62} \\
= \frac{E}{2m} c_4 \int \prod d\tilde{p}_i \tilde{G}_c(\mathbf{p}_1, \mathbf{p}_2) - \int \prod d\tilde{p}_i \tilde{G}_c(\mathbf{p}_1, \mathbf{p}_2) \delta\tilde{V}_{\text{EOM}} \tilde{G}_c(\mathbf{p}_3, \mathbf{p}_4)
\end{aligned}$$

where we defined  $\mathbf{q}_{ij} \equiv \mathbf{p}_i - \mathbf{p}_j$ ,  $q_{ij} \equiv |\mathbf{p}_i - \mathbf{p}_j|$  and

$$\begin{aligned}
\delta\tilde{V}_{\text{EOM}} &= -c_4 \frac{E^2}{4m} (2\pi)^d \delta^{(d)}(\mathbf{q}_{23}) - \left( 2c_4 \alpha_s + 4D_{1,s}^{(2)} \right) \pi C_F \frac{E}{m q_{23}^2} \tag{63} \\
&- \frac{C_F^2 \alpha_s \pi^2}{m q_{23}^{1+2\epsilon}} \left( \alpha_s \frac{c_4}{2} + 2D_{1,s}^{(2)} \right) \frac{e^{\epsilon\gamma_E}}{\mu_s^{-2\epsilon}} \frac{\Gamma^2(\frac{1}{2}-\epsilon)\Gamma(\frac{1}{2}+\epsilon)}{\pi^{3/2}\Gamma(1-2\epsilon)}.
\end{aligned}$$

We thus need the following insertions:

$$\mathcal{I}_l \equiv \int \prod d\tilde{p}_i \tilde{G}_c(\mathbf{p}_1, \mathbf{p}_2) \frac{\log[q_{23}^2/\mu_s^2]}{q_{23}^2} \tilde{G}_c(\mathbf{p}_3, \mathbf{p}_4) \tag{64}$$

$$\mathcal{I}_{l^2} \equiv \int \prod d\tilde{p}_i \tilde{G}_c(\mathbf{p}_1, \mathbf{p}_2) \frac{\log^2[q_{23}^2/\mu_s^2]}{q_{23}^2} \tilde{G}_c(\mathbf{p}_3, \mathbf{p}_4) \tag{65}$$

$$\mathcal{I}_{l,c} \equiv \int \prod d\tilde{p}_i \tilde{G}_c(\mathbf{p}_1, \mathbf{p}_2) \frac{\log[q_{23}^2/\mu_s^2]}{q_{23}^2} \tilde{G}_c(\mathbf{p}_3, \mathbf{p}_4) \frac{1}{q_{45}^2} \tilde{G}_c(\mathbf{p}_5, \mathbf{p}_6) \tag{66}$$

$$\mathcal{I}_{l,l} \equiv \int \prod d\tilde{p}_i \tilde{G}_c(\mathbf{p}_1, \mathbf{p}_2) \frac{\log[q_{23}^2/\mu_s^2]}{q_{23}^2} \tilde{G}_c(\mathbf{p}_3, \mathbf{p}_4) \frac{\log[q_{45}^2/\mu_s^2]}{q_{45}^2} \tilde{G}_c(\mathbf{p}_5, \mathbf{p}_6) \quad (67)$$

$$\mathcal{I}_1 \equiv \int \prod d\tilde{p}_i \tilde{G}_c(\mathbf{p}_1, \mathbf{p}_2) \tilde{G}_c(\mathbf{p}_3, \mathbf{p}_4) \quad (68)$$

$$\mathcal{I}_\delta \equiv \int \prod d\tilde{p}_i \tilde{G}_c(\mathbf{p}_1, \mathbf{p}_2) (2\pi)^{d-1} \delta(\mathbf{p}_2 - \mathbf{p}_3) \tilde{G}_c(\mathbf{p}_3, \mathbf{p}_4) \quad (69)$$

$$\mathcal{I}_{na} \equiv \int \prod d\tilde{p}_i G(\mathbf{p}_1, \mathbf{p}_2) \frac{\mu_s^{2\epsilon}}{q_{23}^{1+2\epsilon}} G(\mathbf{p}_3, \mathbf{p}_4) \quad (70)$$

All these insertions have been computed in Ref. [34]. For the reader's convenience we present the results here. We write them in terms of

$$\ell \equiv \log \left[ -\frac{4mE}{\mu^2} \right] + 2\bar{\psi} \equiv \log \left[ -\frac{4mE}{\mu^2} \right] + 2\psi + 2\gamma_E \quad (71)$$

$$\mathcal{H}_1 \equiv {}_3F_4(1, 1, 1, 1; 2, 2, 1 - \lambda; 1) \quad (72)$$

$$\mathcal{H}_2 \equiv {}_4F_5(1, 1, 1, 1, 1; 2, 2, 2, 1 - \lambda; 1) \quad (73)$$

and the argument of the  $\psi$  functions ( $\psi[x] \equiv d \log \Gamma[x]/dx$ ) and its derivatives is always understood to be  $(1-\lambda) \equiv 1 - (C_F \alpha_s)/(2\sqrt{-E/m})$  unless stated otherwise.

We start by writing the Green function before  $\overline{\text{MS}}$  subtraction

$$\tilde{G}_c(0, 0; E) = \frac{C_F m^2 \alpha_s}{8\pi} \left( \frac{1}{2\epsilon} - \ell - \frac{1}{\lambda} + 1 + \epsilon \mathcal{G}^\epsilon \right), \quad (74)$$

where  $\mathcal{G}^\epsilon$  denotes the term of order  $\epsilon$  of the Green function. This term is not explicitly known, but it is not needed for the calculation of the cross section, even though it results in finite terms in some of the insertions below, because it cancels in the total sum.

The insertions of the higher-order corrections to the Coulomb potential with terms of the form  $\log^j[q^2/\mu_s^2]/q^2$  are computed by taking derivatives with respect to  $\kappa$  at  $\kappa = 0$  of  $\int \prod d\tilde{p}_i \tilde{G}_c(\mathbf{p}_1, \mathbf{p}_2) (q_{23}/\mu_s)^{-2-2\kappa} \tilde{G}_c(\mathbf{p}_3, \mathbf{p}_4)$ . Taking the first derivative yields the insertion of a single logarithm. We get

$$\begin{aligned} \left( \frac{m^2}{64\pi^2} \right)^{-1} \mathcal{I}_l &= \frac{1}{2\epsilon^2} + \frac{1}{\epsilon} - \ell^2 + 4\ell\lambda\psi' \\ &+ 12\psi' - 4\lambda\psi'' - 16\mathcal{H}_1 + 2 - \frac{\pi^2}{4}. \end{aligned} \quad (75)$$

The insertion of a logarithm squared is obtained by taking the second derivative.

$$\begin{aligned} \left( \frac{m^2}{64\pi^2} \right)^{-1} \mathcal{I}_{l^2} &= \frac{1}{2\epsilon^3} + \frac{1}{\epsilon^2} + \frac{2}{\epsilon} + \frac{\pi^2}{12\epsilon} - \frac{2}{3}\ell^3 + 4\ell^2\lambda\psi' \\ &- 8\ell \left( -3\psi' + \lambda\psi'' + 4\mathcal{H}_1 + \frac{\pi^2}{12} \right) \end{aligned} \quad (76)$$

$$\begin{aligned}
& - 16\lambda \psi'^2 - 64\lambda \left( \bar{\psi} + \frac{1}{\lambda} - 2 - \frac{5\pi^2}{48} \right) \psi' - 128 \bar{\psi} \\
& - 32 \left( \frac{2}{3} - \lambda \right) \psi'' + \frac{16}{3} \lambda \psi''' - 128 \mathcal{H}_2 - 64(1 - \bar{\psi}) \mathcal{H}_1 \\
& + 16 S_1 + 52\zeta(3) + 196 + \frac{11\pi^2}{2},
\end{aligned}$$

where

$$S_1 = - \sum_{n=1}^{\infty} \frac{2\Gamma[n]\Gamma[1-\lambda]}{(1+n)^2\Gamma[1+n-\lambda]} \left( 2\bar{\psi}[n] - 2\bar{\psi}[1+n-\lambda] + (1+n)\psi'[1+n] \right). \quad (77)$$

Double insertions of Coulomb potentials are computed in a similar way. The results read

$$\left( \frac{m^2\lambda}{64\pi^3 C_F \alpha_s} \right)^{-1} \mathcal{I}_{l,c} = \ell \left( \psi' - \frac{\lambda}{2} \psi'' \right) - 2\bar{\psi} \psi' + 2\lambda \bar{\psi} \psi'' + \frac{\lambda}{3} \psi''' + 2 S_2, \quad (78)$$

where

$$S_2 = \sum_{n=1}^{\infty} \frac{(n+\lambda)\bar{\psi}[n-\lambda]}{(n-\lambda)^3}, \quad (79)$$

and

$$\begin{aligned}
\left( \frac{m^2\lambda}{64\pi^3 C_F \alpha_s} \right)^{-1} \mathcal{I}_{l,l} &= \ell^2 \left( \psi' - \frac{\lambda}{2} \psi'' \right) + 4\ell \left( \bar{\psi} (\lambda \psi'' - \psi') + \frac{\lambda}{6} \psi''' + S_2 \right) \\
&- \frac{4}{\lambda} \bar{\psi}^3 - 8\lambda \bar{\psi}^2 \psi'' - \frac{8}{\lambda^2} \bar{\psi}^2 \\
&- \frac{8}{\lambda} \bar{\psi} \psi' - 4\bar{\psi} \psi'' - \frac{8}{3} \lambda \bar{\psi} \psi''' - \frac{4}{\lambda^3} \bar{\psi} - \frac{4}{\lambda^2} \psi' \\
&- \frac{2}{\lambda} \psi'' - \frac{2}{3} \psi''' - \frac{\lambda}{6} \psi'''' - 4 S_5 - 8 \bar{\psi} S_2,
\end{aligned} \quad (80)$$

where

$$S_5 = \sum_{n=1}^{\infty} \frac{(n+\lambda)\bar{\psi}[n-\lambda]}{(n-\lambda)^3} \left( -\frac{2\lambda}{n(n-\lambda)} + \frac{2\lambda\bar{\psi}[1-\lambda]}{n} - \frac{(n+\lambda)\bar{\psi}[n-\lambda]}{n} \right). \quad (81)$$

Inserting 1 results in the square of the Green function

$$\mathcal{I}_1 = [G(0, 0; E)]^2. \quad (82)$$

Note that  $\mathcal{I}_1$  obtains a finite contribution due to  $\mathcal{G}^c$ . The insertion due to the  $\delta$  function can be computed directly and takes a very simple form

$$\left( \frac{m\lambda}{4\pi C_F \alpha_s} \right)^{-1} \mathcal{I}_\delta = 2\lambda^2 \psi' + 2\lambda + 1, \quad (83)$$

while the insertion due to the non-analytic potential is more complicated and, written in terms of

$$\bar{\ell} \equiv \ell - 3 + \log 2 \quad (84)$$

reads

$$\begin{aligned} \left(\frac{m^3 C_F \alpha_s}{64\pi^3}\right)^{-1} \mathcal{I}_{na} &= \frac{1}{2\epsilon^2} - \frac{1}{\epsilon} \left(2\bar{\ell} + \frac{2}{\lambda} + 2 - \log 2\right) + 2\bar{\ell}^2 \\ &+ \frac{4\bar{\ell}}{\lambda} + 2\mathcal{G}^\epsilon + 4 - \log^2 2 + 4\log 2 - \frac{5\pi^2}{24} \end{aligned} \quad (85)$$

Finally, the insertion due to the  $L^2$  operator, Eq. (19), can be related to  $\mathcal{I}_{na}$  and  $\mathcal{I}_1$  with the help of Eq. (18) and we get

$$\begin{aligned} \mathcal{I}_{L^2} &\equiv \int \prod d\tilde{p}_i \tilde{G}_c(\mathbf{p}_1, \mathbf{p}_2) \left( \left( \frac{\mathbf{p}_2^2 - \mathbf{p}_3^2}{q_{23}^2} \right)^2 - 1 \right) \tilde{G}_c(\mathbf{p}_3, \mathbf{p}_4) \\ &= \frac{C_F^2 m^4 \alpha_s^2}{2(4\pi)^2} \left( \frac{1}{4\epsilon} - \ell - \frac{1}{2\lambda^2} - \frac{1}{\lambda} + 3 \right) \end{aligned} \quad (86)$$

We are finally in a position to write down the expression for the Green function

$$\begin{aligned} \tilde{G}_{s=1}^{\text{NNLL}} &= \quad (87) \\ &\left(1 - \frac{c_4 E}{2m}\right) \tilde{G}_c \Big|_{\alpha_s \rightarrow \alpha_s} \left( 1 + \frac{E}{2m} c_4 + \frac{E}{m} \frac{D_{1,s}^{(2)}}{\alpha_s} + \frac{\alpha_s}{4\pi} a_1 + \frac{e_Q^2 \alpha_{\text{EM}}}{C_F \alpha_s} + \frac{\alpha_s^2}{(4\pi)^2} a_2 + \frac{C_A^3}{6\beta_0} \alpha_s^2 \log \left[ \frac{\alpha_s(\mu_s)}{\alpha_s(\mu_{us})} \right] \right) \\ &+ i^2 C_F \left( \alpha_s^2 \beta_0 + \frac{\alpha_s^3}{4\pi} (2a_1 \beta_0 + \beta_1) \right) \mathcal{I}_l - i^2 \frac{\alpha_s^3}{4\pi} C_F \beta_0^2 \mathcal{I}_{l^2} \\ &- i^4 2\alpha_s^4 \beta_0 C_F^2 \left( a_1 + \frac{4\pi e_Q^2 \alpha_{\text{EM}}}{C_F \alpha_s^2} \right) \mathcal{I}_{l,c} + i^4 \alpha_s^4 C_F^2 \beta_0^2 \mathcal{I}_{l,l} - i^2 \frac{E^2}{4m} c_4 \mathcal{I}_\delta \\ &+ i^2 \frac{\pi C_F}{m^2} D_{2,s}^{(2)} \mathcal{I}_{L^2} + i^2 \frac{\pi C_F}{m^2} \left( 3D_{d,s}^{(2)} + D_{S^2,s}^{(2)} \frac{(d-4)(d-1)}{d} \right) \mathcal{I}_1 \\ &- i^2 \left( \frac{C_F^2 \alpha_s \pi^2}{2m} (c_4 \alpha_s + 4D_{1,s}^{(2)}) + \frac{C_A C_F \pi^2}{m} (1 - \epsilon) D_s^{(1)} \right) \\ &\quad \times e^{\epsilon\gamma_E} \frac{\Gamma^2(\frac{1}{2} - \epsilon) \Gamma(\frac{1}{2} + \epsilon)}{\pi^{3/2} \Gamma(1 - 2\epsilon)} \mathcal{I}_{na}. \end{aligned}$$

We mention once more that we use strictly expanded results. Thus the terms beyond NNLL that are present in Eq. (87) are dropped.

## B RGI potentials

For ease of reference we explicitly display the RGI potentials not shown in the main body of the paper (we remind that  $\mu_{us} = \mu_s^2/\mu_h$ ):

$$\begin{aligned}
\alpha_{\tilde{V}_s}(\mu_s) &= \alpha_s(\mu_s) \left\{ 1 + \left( a_1 - \beta_0 \log \frac{\mathbf{q}^2}{\mu_s^2} \right) \frac{\alpha_s(\mu_s)}{4\pi} \right. \\
&\quad \left( a_2 - (2a_1\beta_0 + \beta_1) \log \frac{\mathbf{q}^2}{\mu_s^2} + \beta_0^2 \log^2 \frac{\mathbf{q}^2}{\mu_s^2} \right) \frac{\alpha_s^2(\mu_s)}{16\pi^2} \Big\} \\
&\quad + \frac{C_A^3}{6\beta_0} \alpha_s^3(\mu_s) \log \left[ \frac{\alpha_s(\mu_s)}{\alpha_s(\mu_{us})} \right], \tag{88}
\end{aligned}$$

$$D_s^{(1)}(\mu_s) = \alpha_s^2(\mu_s) \left\{ 1 + \frac{16}{3\beta_0} \left( \frac{C_A}{2} + C_F \right) \log \left[ \frac{\alpha_s(\mu_s)}{\alpha_s(\mu_{us})} \right] \right\},$$

$$D_{1,s}^{(2)}(\mu_s) = \alpha_s(\mu_s) \left\{ 1 + \frac{8C_A}{3\beta_0} \log \left[ \frac{\alpha_s(\mu_s)}{\alpha_s(\mu_{us})} \right] \right\},$$

$$D_{2,s}^{(2)}(\mu_s) = \alpha_s(\mu_s),$$

$$D_{S^2,s}^{(2)}(\mu_s) = \alpha_s(\mu_s) c_F^2(\mu_s) - \frac{3}{2\pi C_F} (d_{sv}(\mu_s) + C_F d_{vv}(\mu_s)),$$

$$D_{LS,s}^{(2)}(\mu_s) = \frac{\alpha_s(\mu_s)}{3} (c_S(\mu_s) + 2c_F(\mu_s)),$$

$$D_{S_{12},s}^{(2)}(\mu_s) = \alpha_s(\mu_s) c_F^2(\mu_s),$$

where  $(z = \left[ \frac{\alpha_s(\mu_s)}{\alpha_s(\mu_h)} \right]^{\frac{1}{\beta_0}} \simeq 1 - 1/(2\pi)\alpha_s(\mu_s) \log(\frac{\mu_s}{\mu_h}), \beta_0 = \frac{11}{3}C_A - \frac{4}{3}T_F n_f)$

$$c_F(\mu_s) = z^{-C_A},$$

$$c_S(\mu_s) = 2z^{-C_A} - 1,$$

$$\begin{aligned}
c_D(\mu_s) &= \frac{9C_A}{9C_A + 8T_F n_f} \left\{ -\frac{5C_A + 4T_F n_f}{4C_A + 4T_F n_f} z^{-2C_A} + \frac{C_A + 16C_F - 8T_F n_f}{2(C_A - 2T_F n_f)} \right. \\
&\quad + \frac{-7C_A^2 + 32C_A C_F - 4C_A T_F n_f + 32C_F T_F n_f}{4(C_A + T_F n_f)(2T_F n_f - C_A)} z^{4T_F n_f/3 - 2C_A/3} \\
&\quad \left. + \frac{8T_F n_f}{9C_A} \left[ z^{-2C_A} + \left( \frac{20}{13} + \frac{32}{13} \frac{C_F}{C_A} \right) \left[ 1 - z^{-\frac{13C_A}{6}} \right] \right] \right\},
\end{aligned}$$

$$\begin{aligned}
\frac{d_{ss}(\mu_s)}{C_F} + d_{vs}(\mu_s) &= -(2C_F - 3C_A) \frac{2\pi}{\beta_0} \alpha_s(\mu_h) [z^{\beta_0} - 1] \\
&\quad - \frac{27C_A^2}{9C_A + 8T_F n_f} \frac{\pi}{\beta_0} \alpha_s(\mu_h) \left\{ -\frac{5C_A + 4T_F n_f}{4C_A + 4T_F n_f} \frac{\beta_0}{\beta_0 - 2C_A} (z^{\beta_0 - 2C_A} - 1) \right. \\
&\quad + \frac{C_A + 16C_F - 8T_F n_f}{2(C_A - 2T_F n_f)} (z^{\beta_0} - 1) \\
&\quad + \frac{-7C_A^2 + 32C_A C_F - 4C_A T_F n_f + 32C_F T_F n_f}{4(C_A + T_F n_f)(2T_F n_f - C_A)} \\
&\quad \left. \times \frac{3\beta_0}{3\beta_0 + 4T_F n_f - 2C_A} (z^{\beta_0 + 4T_F n_f/3 - 2C_A/3} - 1) \right\}
\end{aligned}$$

$$\begin{aligned}
& + \frac{8T_F n_f}{9C_A} \left[ \frac{\beta_0}{\beta_0 - 2C_A} (z^{\beta_0 - 2C_A} - 1) + \left( \frac{20}{13} + \frac{32 C_F}{13 C_A} \right) \right. \\
& \quad \left. \times \left( [z^{\beta_0} - 1] - \frac{6\beta_0}{6\beta_0 - 13C_A} [z^{\beta_0 - \frac{13C_A}{6}} - 1] \right) \right] \Bigg\} , \\
\frac{d_{sv}(\mu_s)}{C_F} + d_{vv}(\mu_s) & = \frac{C_A}{\beta_0 - 2C_A} \pi \alpha_s(\mu_h) \left\{ z^{\beta_0 - 2C_A} - 1 \right\} . \tag{89}
\end{aligned}$$

## References

- [1] V. S. Fadin and V. A. Khoze, JETP Lett. **46**, 525 (1987) [Pisma Zh. Eksp. Teor. Fiz. **46**, 417 (1987)];  
V. S. Fadin and V. A. Khoze, Sov. J. Nucl. Phys. **48**, 309 (1988) [Yad. Fiz. **48**, 487 (1988)].
- [2] M. Martinez and R. Miquel, Eur. Phys. J. C **27**, 49 (2003) [arXiv:hep-ph/0207315].
- [3] A. H. Hoang *et al.*, Eur. Phys. J. directC **2**, 1 (2000) [arXiv:hep-ph/0001286].
- [4] V. A. Novikov *et al.*, Phys. Rev. Lett. **38**, 626 (1977) [Erratum-ibid. **38**, 791 (1977)]; V. A. Novikov *et al.*, Phys. Rept. **41**, 1 (1978).
- [5] K. Melnikov and A. Yelkhovsky, Phys. Rev. **D59** 114009 (1999).
- [6] A. A. Penin and A. A. Pivovarov, Nucl. Phys. B **549**, 217 (1999) [arXiv:hep-ph/9807421].
- [7] A. H. Hoang, Phys. Rev. D **59**, 014039 (1999) [arXiv:hep-ph/9803454];  
A. H. Hoang, Phys. Rev. D **61**, 034005 (2000) [arXiv:hep-ph/9905550].
- [8] M. Beneke and A. Signer, Phys. Lett. B **471** (1999) 233 [arXiv:hep-ph/9906475].
- [9] A. Pineda and A. Signer, Phys. Rev. D **73**, 111501 (2006) [arXiv:hep-ph/0601185].
- [10] N. Brambilla, A. Pineda, J. Soto and A. Vairo, Rev. Mod. Phys. **77**, 1423 (2005).
- [11] M. Beneke and V. A. Smirnov, Nucl. Phys. B **522**, 321 (1998) [arXiv:hep-ph/9711391].
- [12] W. E. Caswell and G. P. Lepage, Phys. Lett. B **167**, 437 (1986).



- [13] A. Pineda and J. Soto, Nucl. Phys. Proc. Suppl. **64**, 428 (1998) [arXiv:hep-ph/9707481];  
A. Pineda and J. Soto, Phys. Rev. D **59**, 016005 (1999) [arXiv:hep-ph/9805424].
- [14] N. Brambilla, A. Pineda, J. Soto and A. Vairo, Nucl. Phys. B **566**, 275 (2000) [arXiv:hep-ph/9907240].
- [15] N. Brambilla, A. Pineda, J. Soto and A. Vairo, Phys. Rev. D **60**, 091502 (1999) [arXiv:hep-ph/9903355].
- [16] B. A. Kniehl and A. A. Penin, Nucl. Phys. B **563**, 200 (1999) [arXiv:hep-ph/9907489];  
B. A. Kniehl and A. A. Penin, Nucl. Phys. B **577**, 197 (2000) [arXiv:hep-ph/9911414].
- [17] N. Brambilla, A. Pineda, J. Soto and A. Vairo, Phys. Lett. B **470**, 215 (1999) [arXiv:hep-ph/9910238].
- [18] B. A. Kniehl, A. A. Penin, M. Steinhauser and V. A. Smirnov, Phys. Rev. D **65**, 091503 (2002) [arXiv:hep-ph/0106135].
- [19] A. A. Penin, V. A. Smirnov and M. Steinhauser, Nucl. Phys. B **716**, 303 (2005) [arXiv:hep-ph/0501042].
- [20] M. Beneke, Y. Kiyo and K. Schuller, Nucl. Phys. B **714**, 67 (2005) [arXiv:hep-ph/0501289].
- [21] P. Marquard, J. H. Piclum, D. Seidel and M. Steinhauser, arXiv:hep-ph/0607168.
- [22] A. Pineda, Phys. Rev. D **65**, 074007 (2002) [arXiv:hep-ph/0109117].
- [23] A. H. Hoang and I. W. Stewart, Phys. Rev. D **67**, 114020 (2003) [arXiv:hep-ph/0209340].
- [24] B. A. Kniehl, A. A. Penin, A. Pineda, V. A. Smirnov and M. Steinhauser, Phys. Rev. Lett. **92**, 242001 (2004) [arXiv:hep-ph/0312086].
- [25] A. A. Penin, A. Pineda, V. A. Smirnov and M. Steinhauser, Phys. Lett. B **593**, 124 (2004) [arXiv:hep-ph/0403080].
- [26] A. Pineda, Phys. Rev. D **66** (2002) 054022 [arXiv:hep-ph/0110216].
- [27] A. A. Penin, A. Pineda, V. A. Smirnov and M. Steinhauser, Nucl. Phys. B **699**, 183 (2004) [arXiv:hep-ph/0406175].

- [28] A. H. Hoang, A. V. Manohar, I. W. Stewart and T. Teubner, Phys. Rev. Lett. **86**, 1951 (2001) [arXiv:hep-ph/0011254].
- [29] A. H. Hoang, A. V. Manohar, I. W. Stewart and T. Teubner, Phys. Rev. D **65**, 014014 (2002) [arXiv:hep-ph/0107144].
- [30] M. E. Luke, A. V. Manohar and I. Z. Rothstein, Phys. Rev. D **61**, 074025 (2000) [arXiv:hep-ph/9910209].
- [31] I. I. Y. Bigi, M. A. Shifman and N. Uraltsev, Ann. Rev. Nucl. Part. Sci. **47**, 591 (1997) [arXiv:hep-ph/9703290];  
A. H. Hoang, Z. Ligeti and A. V. Manohar, Phys. Rev. Lett. **82**, 277 (1999) [arXiv:hep-ph/9809423].
- [32] M. Beneke, Phys. Lett. B **434**, 115 (1998) [arXiv:hep-ph/9804241].
- [33] A. Pineda, JHEP **0106** (2001) 022 [arXiv:hep-ph/0105008].
- [34] M. Beneke, A. Signer and V. A. Smirnov, Phys. Lett. B **454**, 137 (1999) [arXiv:hep-ph/9903260].
- [35] M. Beneke, arXiv:hep-ph/9911490.
- [36] A. Czarnecki and K. Melnikov, Phys. Rev. Lett. **80**, 2531 (1998) [arXiv:hep-ph/9712222];  
M. Beneke, A. Signer and V. A. Smirnov, Phys. Rev. Lett. **80**, 2535 (1998) [arXiv:hep-ph/9712302].
- [37] A. Czarnecki and K. Melnikov, Phys. Lett. B **519**, 212 (2001) [arXiv:hep-ph/0109054].
- [38] Y. Schroder, Phys. Lett. B **447**, 321 (1999) [arXiv:hep-ph/9812205];  
M. Peter, Phys. Rev. Lett. **78**, 602 (1997) [arXiv:hep-ph/9610209].
- [39] A. Pineda and J. Soto, Phys. Lett. B **495**, 323 (2000) [arXiv:hep-ph/0007197].
- [40] G. T. Bodwin, E. Braaten and G. P. Lepage, Phys. Rev. D **51**, 1125 (1995) [Erratum-ibid. D **55**, 5853 (1997)] [arXiv:hep-ph/9407339].
- [41] N. Brambilla, D. Eiras, A. Pineda, J. Soto and A. Vairo, Phys. Rev. D **67**, 034018 (2003) [arXiv:hep-ph/0208019].
- [42] A. P. Chapovsky, V. A. Khoze, A. Signer and W. J. Stirling, Nucl. Phys. B **621**, 257 (2002) [arXiv:hep-ph/0108190];  
M. Beneke, A. P. Chapovsky, A. Signer and G. Zanderighi, Phys. Rev. Lett. **93**, 011602 (2004) [arXiv:hep-ph/0312331];

- M. Beneke, A. P. Chapovsky, A. Signer and G. Zanderighi, Nucl. Phys. B **686**, 205 (2004) [arXiv:hep-ph/0401002].
- [43] V. S. Fadin, V. A. Khoze and A. D. Martin, Phys. Rev. D **49**, 2247 (1994);  
V. S. Fadin, V. A. Khoze and A. D. Martin, Phys. Lett. B **320**, 141 (1994)  
[arXiv:hep-ph/9309234];  
K. Melnikov and O. I. Yakovlev, Phys. Lett. B **324**, 217 (1994)  
[arXiv:hep-ph/9302311].
- [44] A. H. Hoang and C. J. Reisser, Phys. Rev. D **71**, 074022 (2005)  
[arXiv:hep-ph/0412258].
- [45] A. H. Hoang, Phys. Rev. D **69**, 034009 (2004) [arXiv:hep-ph/0307376].